Nuclear Inst. and Methods in Physics Research, A 926 (2019) 101–117

Contents lists available at ScienceDirect

Nuclear Inst. and Methods in Physics Research, A

journal homepage: www.elsevier.com/locate/nima

Silicon Photomultipliers and SPAD imagers in biophotonics: Advances and perspectives

M. Caccia [a,*], L. Nardo [a], R. Santoro [a], D. Schaffhauser [b]

[a] Universitá dell'Insubria, Dipartimento di Scienza ed Alta Tecnologia, Via Valleggio 11, 22100 Como, Italy
[b] rqmicro AG, Brandstrasse 24, 8952 Schlieren, Switzerland

ARTICLE INFO

Keywords:
Biophotonic techniques
Silicon Photomultipliers
SPAD imagers

ABSTRACT

Photonics is essential in life science research and the continuous development of methods offers researchers tools of unprecedented sensitivity. Sensors are key to the exploitation of the most advanced biophotonic techniques with highly demanding specifications in terms of single photon sensitivity, time resolution, miniaturisation real-time processing and data throughput. Silicon photomultipliers and Single Photon Avalanche Diode (SPAD) imagers represent the state-of-the-art in photon detection with single photon sensitivity, photon number resolving capability and the possibility to integrate on chip advanced functionalities. As a consequence, they can be the platform for the next generation biophotonic instruments and methods.

This paper summarises the main biophotonic techniques and reports exemplary applications of Silicon Photomultipliers and SPAD imagers for fluorescence, chemiluminescence, time correlated single photon counting and imaging. Achievements and current limitations are addressed, pointing as well to the most recent technology advances and highlighting the possible pathways for the near future.

Contents

1. Introduction

Biophotonics is the set of methods and techniques aiming at gaining knowledge of biological systems at molecular, cellular and systemic level by emitted, absorbed and scattered light. It is an extremely complex and cross-disciplinary branch of Science, requiring high level expertise in cell and molecular biology, biochemistry, physics in general, optics and optical technologies, sensing, analog and digital electronics and, last but not least, data handling and advanced analysis techniques. Sensors are essential and, irrespective from the fact that the majority of biophotonic instruments on the market are still today based on Photo-Multiplier Tubes (PMT), it is certainly true that silicon based detectors, notably Single Photon Avalanche Diodes (SPAD), Scientific CMOS Cameras (sCMOS) and Electron Multiplying CCD (EMCCD) were

* Corresponding author.
E-mail address: massimo.caccia@uninsubria.it (M. Caccia).

https://doi.org/10.1016/j.nima.2018.10.204
Received 26 June 2018; Received in revised form 8 October 2018; Accepted 29 October 2018
Available online 26 November 2018
0168-9002/

key to the development of advanced techniques. However, the use of Silicon Photomultipliers (SiPM), generically meant as arrays of SPAD with a single output, is lagging behind. Irrespective from the impressive technology development, the impact of SiPM in biophotonics has been so far marginal, with a limited number of documented proofs-of-concept and very few products on the market. On the other hand, as the single cells of the sensor are indexed turning them into single photon sensitive pixels (SPAD imagers) and complex functionalities are implemented on chip, advantages become more clear. Even if this class of sensors has been so far mainly used in the research domain, the development is rapidly achieving its maturity making them interesting for the market.

For the benefit of the target community, this paper addresses a non-exhaustive introduction to biophotonic techniques in Section 2, with a focus on the basic requirements and the state-of-the-art. This is followed by an analysis of exemplary illustrations of the use of SiPM and SPAD arrays in CMOS technology, in Section 3. The authors' view on the way forward closes the paper.

2. A short guide to biophotonic techniques

Biophotonic techniques can be divided in two classes, depending on whether the signal results by spontaneous luminescence of the biological sample under investigation or by the interaction of the sample with an external source of light. In the first instance, light is generated by photochemical reactions, either metabolic (bioluminescence [1]) or due to the reactivity of exogenous molecules with metabolites or biologically relevant molecules including ions and reactive oxygen species (chemiluminescence [2]). The second class of techniques is more heterogeneous. Upon interacting with the biological sample, light can be either transmitted [3,4], absorbed [5–7], or scattered [7–11]. Moreover, light absorption may result in re-emission at different wavelength by molecules within the sample, by means of either fluorescence [12,13] or phosphorescence [13–15].

Another key to classify biophotonic techniques, possibly more relevant here, relies on the observables in the light signal detection process. According to this scheme, three main procedures can be identified: light intensity measurements, single-photon counting and time-correlated single-photon counting. For every procedure, both point-like and spatially resolved techniques have been developed.

2.1. Light intensity measurements

In light intensity measurements, the signal is expected to vary over a rather extended range which typically spans at least six orders of magnitude. For instance, in standard metabolite detection/quantification assays, the most common applications, the metabolite concentrations vary from nanomolar to millimolar. The photon fluxes rarely occur to be weaker than several hundred photons per second per squared centimetre in spontaneous luminescence based assays. In assays based on an external light source, the detector sensitive area is illuminated by a number of photons exceeding tens of millions per second for an incoming light intensity typically limited to 10^{-5} W/cm^2. The baseline detectors for these measurements are PMT used in current mode or Avalanche PhotoDiodes (APD) on the low intensity side and photodiodes for higher intensities. Among the most popular techniques, it is worth quoting in vitro absorption and fluorescence analyses of single specimen (e.g., held in cuvette [16,17]) and more sophisticated high-throughput screening procedures based on multi-well plates [18–23] or micro-array [24–26] scanning.

Most of these assays essentially consist in the detection of a given (bio)molecular species of interest and the measurement of its concentration. In this respect, the fluorescence signal offers higher sensitivity (down to picomolar) with respect to absorption techniques. However it requires a careful calibration to determine absolute concentration values [27], where calibration-free absorption wins in the micromolar-to-millimolar range [28]. Moreover, since absorption occurs on time scales shorter than femtoseconds and fluorescence is typically emitted a few nanoseconds after the excitation, the latter is more affected by environmental properties and molecular interactions [29], which can be exploited to probe the environment [30] but decreases the reproducibility of the measurements in quantitation experiments [31].

Low throughput analyses made in cuvette on single/few samples are most often used to characterise single metabolic reactions at the molecular level in a simplified environment. In binding reactions between small ligand molecules (e.g., drugs or metabolites) and biological macromolecules such as proteins [32,33] or nucleic acids [34] the electronic configuration of the ligand is extensively affected, so that the energy levels involved in both absorption and fluorescence emission are perturbed. The fraction of ligand bound to the macromolecule can be measured by the changes of its absorption or fluorescence at varying the macromolecule concentration.

If the reaction to be monitored involves the binding between molecules of comparable size (e.g.: protein–protein or protein–nucleic acids interactions), one solution is to label one or both reactants with exogenous fluorophores and to exploit a phenomenon called Fluorescence Resonance Energy Transfer (FRET) [35–37]. This is a quantum resonance occurring between an excited fluorophore (the donor) and a nearby dye (the acceptor) whose absorption spectrum is significantly overlapped to the emission spectrum of the donor. As a result of this resonance, the excitation energy is transferred from the donor, which is brought back to the ground state without emitting fluorescence light, to the acceptor, which is promoted to the excited state and emits fluorescence light in a red-shifted band with respect to the donor emission wavelength. This phenomenon scales with the inverse of the donor-to-acceptor distance to the sixth power. Assuming that the sample is excited with light in the absorption band of the donor, as the two reactants are separate in solution (unbound state) they will produce negligible FRET. Conversely, as they bind the chromophores labelling them are separated by a few nanometres at most and FRET is dominant. Thus, progressive quenching of the donor fluorescence and simultaneous increase in acceptor fluorescence reveals the development of the binding reaction [38].

High throughput screening is essentially based on multi-well plate readers, featuring a variety of detection modes for different assays [39–43]. Among them, it is worth mentioning the ELISA technique (Enzyme-Linked Immuno-Sorbent Assay) [44–46] and DNA micro-arrays, identifying the presence of a particular panel of DNA sequences within a biological sample [24–26]. In order to do so, probe DNA oligonucleotides with sequences complementary to the ones to be detected are linked to the well surface, with a different sequence per well. The DNA (or RNA) under test is subject to amplification of the region of interest by means of Polymerase Chain Reaction (PCR) [47], and the PCR products are labelled and deposited in each well. After a waiting time tuned to let the DNA react with the probes, the wells are rinsed and the plate is scanned for measuring the fluorescence intensity. In their simplest form, multi-well analysis methods are qualitative, providing a map of the probed specimen by the enlighted wells. The system can be made quantitative using solutions containing any analyte of interest in known concentrations to obtain a calibration curve.

Chemiluminescence is also exploited to monitor specific reactions or quantify selected metabolites by plate-reading analyses [48,49]. An example is detection of calcium spikes in cells [50–53]. Calcium is an ubiquitous second-level signalling effector. Recognition of a ligand outside the cell by a receptor on the cell surface (typically a transmembrane protein) triggers either calcium influx from the extracellular medium or secretion of calcium stored in the endoplasmic reticulum. This calcium gradient further activates a cascade of reactions. Several chemiluminescent assays (including luciferase and aequorin based assays) are sensitive to calcium concentration. The specimens of election for chemiluminescence-based plate-reading assays are cells cultured within the plate wells. The cells must be suitably transfected to express the desired chemiluminescent proteins. Nowadays, there exist plate

reading instrumentation of any costs ranging from few thousands to more than one hundred thousand dollars, allowing to read a variety of multi-well plates (Fig. 1). The latter have standardised dimensions of 12.776×8.548 cm^2 to be compliant with all commercial plate readers. The number of wells varies from 6 to as many as 1536, although the most widespread plates host 24 or 96 wells. The wells are arranged on a rectangular array and the mounting stage submits sequentially all the wells to illumination by a single light beam. The detector, which is typically facing the source, is a standard photodiode or photomultiplier tube usually interfaced with a band-pass filter cutting the excitation light in case of fluorescence-based assays. The main technological advances aim to speeding up the reading process through either reduction of the dwell time (currently at the level of few seconds/well) or parallelising the procedure [54]. Reducing the acquisition time would not only be desirable on a practical standpoint but is an indispensable requirement whenever the biological samples under investigation are degradable or dynamic.

In many fields of biology and medicine, flow cytometry, namely the multi-parametric characterisation of cells suspended in a stream of fluid, has been proven to be a fast and reliable method [55–57]. Initially targeted towards eukaryotic cells, technical advancements in fluidics, optics and electronics have made the detection of sub-micrometric cells possible. This enabled flow cytometry to be used in new fields of application such as microbiology [58–60]. Crucial to the performance of flow cytometers are the optical detectors which must be able to resolve weak signals, down to 10^{-9} W/cm^2 at the detector, at frequencies up to 10^6 Hz. Ever since the commercial inception of flow cytometry methods (FCM) in the early 1970s, these instruments have therefore predominantly been equipped with PMT. However, with the rise of APD technology, manufacturers of flow cytometers have looked into replacing PMT with high gain silicon based light sensors [61–64].

Traditional flow cytometers [65] make use of an optical set-up which is designed around a permanently built-in flow cell carrying the liquid sample (Fig. 2). Typical dimensions of the flow cell are several 100 μm in height and width with volumetric flow rates in the range of 10 to 1000 μl/min. In most cases, one or more lasers are used for illumination of the samples inside the flow cell with a focal size between 5 and 50 μm. In order to ensure that all cells pass through the focal spot, hydrodynamic focusing is used. With the aforementioned design parameters a sample of 1 ml can be analysed within several minutes. Modern flow cytometers are able to reliably detect cell flow rates up to 100 000 per second; in more advanced systems, distinction of different cell populations may be implemented by real time separation of specific subtypes. This practice is referred to as cell sorting [66,67].

Typical information gained from a single detection event are cell size, morphology and the fluorescence produced by fluorochromized antibodies recognising membrane receptors. The former two attributes are usually measured by dynamic light scattering using conventional photodiodes due to the strong optical signal. Fluorescence allows to classify different subtypes within a cell population. However the signal is usually much weaker with respect to scattered light, requiring the use of PMT. Often, several different fluorescence signals are obtained simultaneously, sometimes even excited using the same laser. This makes spectral splitting of the emitted light necessary, requiring many optical elements such as lenses, dichroic mirrors and filters. The individual light beams are then collected by individual sensors. One of the main challenges in the optical design is the back-reflected laser light which often has an intensity several orders of magnitude higher than the fluorescence signal. This requires the use of state-of-art dielectric filters with optical densities higher than 6, which are mostly implemented as discrete elements in front of the detectors. The combination of these design constraints usually results in large and expensive set-ups with a limited flexibility.

A valuable alternative to spectral separation of different labels, virtually allowing to use a single detector to discriminate the emission of fluorophores with overlapping excitation and emission spectra, consists in tagging each label by its fluorescence lifetime (*vide infra*) [69–72].

2.2. Photon counting techniques

Biophotonic techniques based on the detection of fluorescence photons emitted by a single or a low plurality of molecules have a primary importance [73]. However, they are rather limited to the academic practice due to their niche application. All of these techniques aim at the reconstruction of the distribution of the number of photons in predefined time bins. The frequency of the emitted photons is typically at the MHz level for every molecule in the observation volume, for excitation intensities of 100 μW, limited to avoid tissue photo-damage. The main applications address Fluorescence Correlation Spectroscopy (FCS) [74–79], the reconstruction of Photon Counting Histograms (PCH) [80–84] and single molecule FRET [37,85,86].

FCS essentially consists in the reconstruction of the autocorrelation function of the fluorescence signal, where fluctuations are expected because of the variations in the number of fluorophores within an observation volume of fractions of femtoliter [87]. Such a tiny spot can be obtained by either of three well consolidated techniques: confocal excitation/detection geometry [88,89], total internal reflection fluorescence excitation [86,90], or multiphoton fluorescence excitation [89,91]. A typical FCS set-up, exploiting confocal geometry, is sketched in Fig. 3. Fluctuations are primarily connected to the particle typical dwell time, namely the time spent within the observation volume, which in turn is linked to the diffusion coefficient, depending on the hydrodynamic radius of the diffusing particle, affected by the shape and the mass. The typical dwell time ranges between 30 μs for a fluorophore to 500 μs for a large protein. Presuming a Poisson distribution in the number of molecules within the observation volume, the ratio between the r.m.s. fluctuations of the fluorescence and the average intensity scales as the square root of the average number of fluorophores. As a consequence, the value of the autocorrelation function tends to 1/N for delay time approaching zero, where N is the average number of fluorophore molecules. Thus, upon calibration of the observation volume size, FCS provides as well a measurement of the fluorophore local concentration with sensitivity down to the femtomolar regime. FCS has been successfully applied in a variety of investigations, e.g. to monitor the dynamics of protein quaternary structure, binding interactions, bending of DNA fragments due to interaction with proteins and protein conformational transitions [92,93].

In the late 1990's, Gratton and coworkers proposed an alternative method to exploit fluorescence fluctuations, based on the analysis of the Photon Counting Histogram (PCH), namely the distribution of the number of detected photons in a pre-defined time interval [80]. The probability density function is expected to be Poissonian in case of emission by a fixed number of fluorophores. Randomness in the number of detected photons results by the excitation laser intensity fluctuations, the binomial distribution accounting for the photon detection efficiency and the intrinsically stochastic nature of the fluorescence emission process. However, in the case of few freely diffusing molecules, further fluctuations in the photon number are induced by the non-homogeneous excitation beam intensity profile and the stochastic variations in the number of molecules in the observation volume. This makes the PCH super-Poissonian. When $N \leq 1$, deviations become sizeable in the high photon number tail of the distribution, for photon number probabilities lower than 10^{-3}. A moment-based analysis of the PCH leads to the measurement of the local concentration and molecular brightness of a fluorophore, namely the expectation value of the number of fluorescence photons per molecule per time bin. More precise information, including separation of the contribution of different species in a fluorophore mixture, can be obtained by fitting the distribution to analytical models, although the latter are non-trivial.

In its simplest embodiment, Single-Molecule FRET (SM-FRET) is applied to freely diffusing molecules [94]. The principle and the set-up are similar to what is described for fluorescence fluctuation spectroscopy experiments, with the main difference of integrating a dichroic mirror separating fluorescence by the donor and the acceptor. In order to

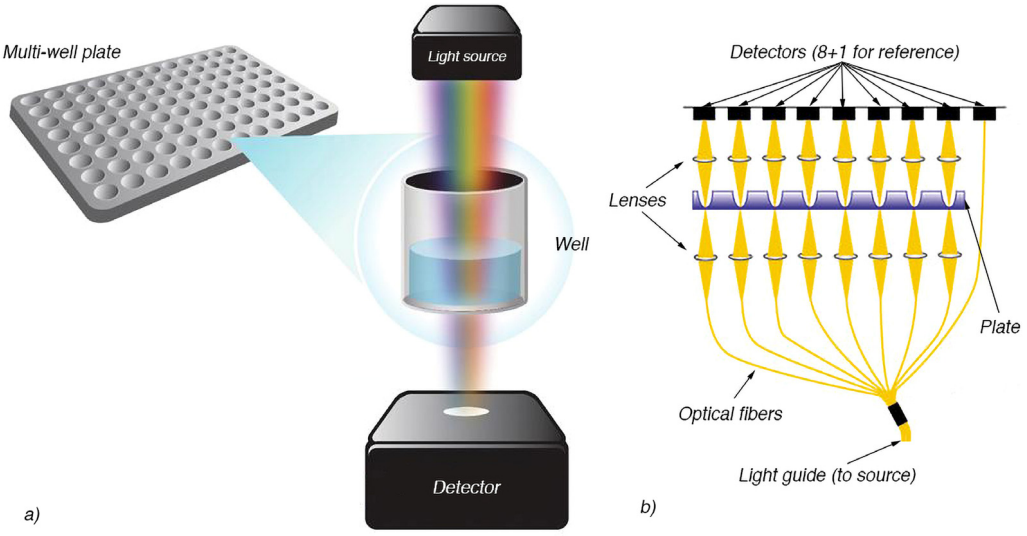

Fig. 1. The main components of a multi-well plate reading set-up. (a) Illumination detection set-up configuration. (b) Scheme of parallelised plate reading.
Source: Reproduced from [54].

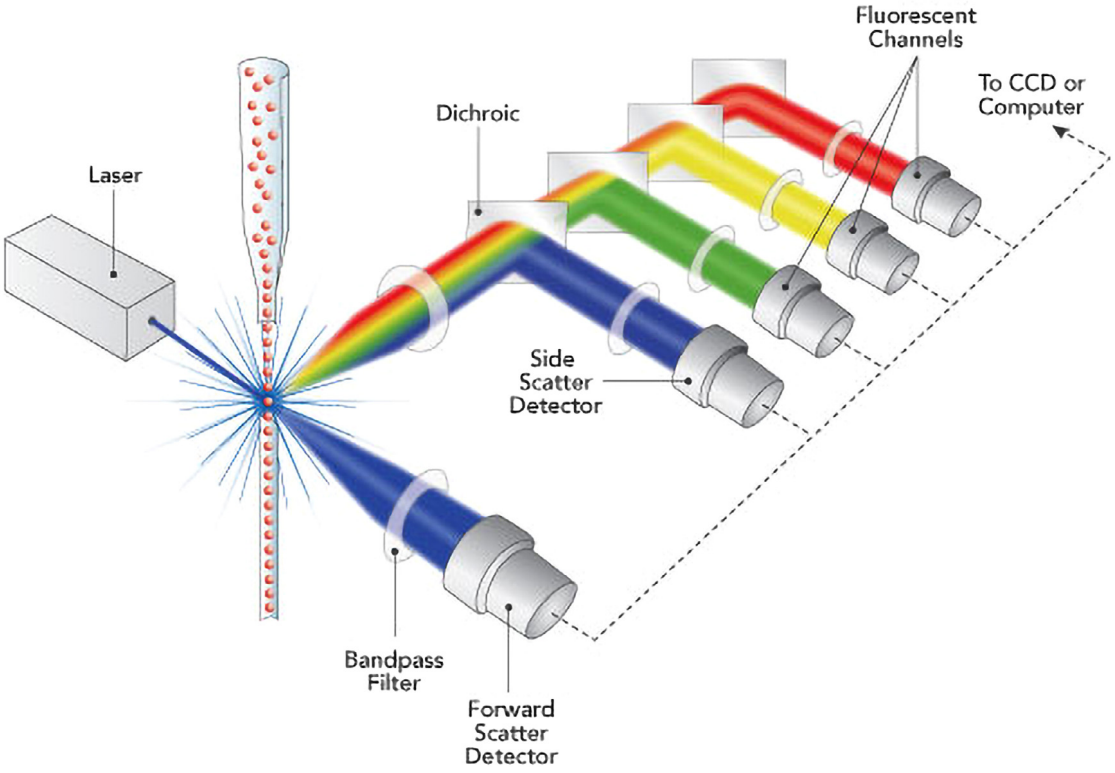

Fig. 2. Scheme of the flow cell and optical set-up of a cytometer.
Source: Reproduced from [68].

operate in single molecule regime, the expectation value of the number of fluorophores in the observation volume must not exceed 1/10, according to the golden rule reported in [86]. If so, when a single molecule dual-labelled with a donor–acceptor pair transits across the observation volume, it is excited and emits fluorescence several times during its dwell time, thus giving birth to a photon burst in both the donor and acceptor detection channels. The ratio between the two intensities is retained as a measurement of the conformation of the molecule of interest. Building an histogram of the values assumed by the ratio allows discriminating among different conformations which are reflected in a multimodal distribution. This is the main advantage of the technique with respect to bulk FRET, where only the average donor-to-acceptor distance is measured.

Until now, FCS, PCH and SM-FRET have been performed relying on SPAD or single-photon sensitive PMT detectors. In order to avoid a bias due to the signal pile-up, measurements are performed limiting the count rate during photon bursts to few hundreds of kHz, much below the photodamage threshold. Accordingly, in order to have a significant

dynamic range in the number statistics, it is necessary to sample at rather long time bins (10 microseconds or more). Obviously, this sets a lower limit on the sensitivity to fluorescence fluctuations and conformational dynamics occurring on time scales comparable or even shorter than the sampling time. Notably, many biologically relevant phenomena liable to affect the fluorescence intensity take place at the sub-microsecond time scale [94,95], representing a major challenge towards further implementation of these otherwise consolidated techniques.

Beside fluorescence based methods, it is worth mentioning functional near-infrared (NIR) spectroscopy [6,96], another technique requiring sensitivity to a low plurality of photons. Although not routinely applied in clinical practice yet, it appears to be very promising. The method consists in illuminating a portion of tissue with laser at two different wavelengths in the red (around 680 nm) and IR region (around 850 nm) and measure the back-scattered light emerging from the tissue at a distance of few-to-several centimetres from the illumination spot. Because the red light is absorbed by oxidised haemoglobin, while the NIR radiation is absorbed by deoxy-haemoglobin, detecting the ratio of red-to-NIR light re-emerging from the tissue allows the estimation of the O_2 saturation of the probed tissue. Functional NIR spectroscopy measurements in the brain are of particular interest, as the fraction of oxy-hemoglobine measured at a spot is significant of the local cortical activity. Moreover, this technique, relying on low doses of non-ionising radiation, is minimally invasive. Finally, the wavelengths exploited to monitor hemoglobin have a rather high penetration depth within tissues. As of today, single photon sensitive PMT are used. However, they lack the features enabling the exploitation of this technique in everyday clinical practice. In particular, the ambition is to construct wearable equipment capable of monitoring neuronal activity in every-day life. Moreover, functional NIR spectroscopy in synergy with nuclear magnetic resonance without contrast medium would allow to get brain images endowed with optimal spatial resolution coupled with valuable information on local neuronal activity.

2.3. Time correlated single photon counting

Time stamped detection of single photons is massively applied in academic as well as industrial research to reconstruct fluorescence decay patterns in time-resolved fluorescence spectroscopy and photon time of flight distributions in optical tomography and optical biopsy. An exhaustive synopsis is beyond the scope of this review and we will only outline the main technical features and quote two basic applications, referring to [97] for a comprehensive overview. In typical time-correlated single-photon counting (TCSPC) experiments (see Fig. 4), the sample is irradiated with a periodic train of picosecond long light pulses with repetition rates in the range of several tens of megahertz. Time stamping and recording the arrival of photons from the sample, the temporal profile of the light pulse of interest can be reconstructed. The intensity of the excitation beam is tuned to comply with the so-called single photon regime, where the probability of having more than one photon per pulse impinging on the detector must be statistically negligible, in order to minimise the signal pile-up [97], biasing the measurement. Nowadays, the technique is essentially based on PMT and SPAD, because of their single-photon sensitivity, time resolution (20–30 ps at best) and low dark count rate (tens of Hz for SPAD, even lower for PMT). However, because of the dead-time due to both the sensor and the time digitisation circuitry, the photon rate, namely the average number of detected photons per excitation pulse, cannot exceed 0.05. This can be actually considered the major limitation in present systems.

Time-resolved fluorescence measurements offer several advantages with respect to methods based on the fluorescence intensity. Both intensity and lifetime are sensitive to environment, reactivity, conformation of the fluorophore and of the biomolecules interacting with it. However, while intensity is strongly concentration sensitive and its measurement is potentially affected by spurious light, the fluorescence lifetime is not affected by these undesired biases. As such, it results a more robust

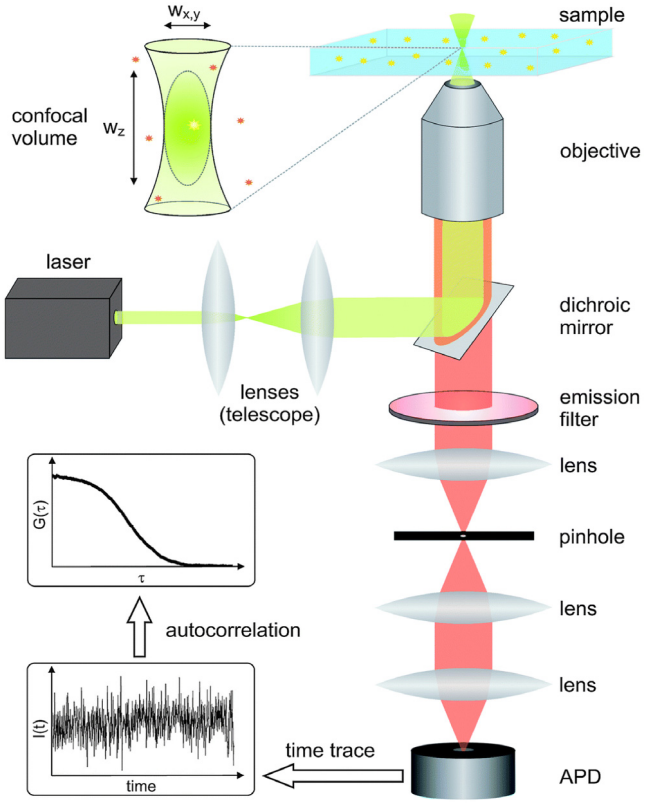

Fig. 3. Scheme of a fluorescence correlation spectroscopy set-up. In the picture, the femtoliter-sized observation volume is obtained by confocal excitation/detection geometry.

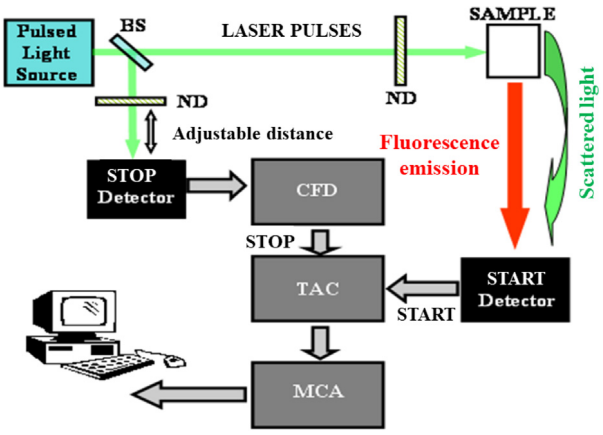

Fig. 4. The building blocks of a typical Time-Correlated Single-Photon Counting set-up. Because of the low photon rate, time stamping of the pulses usually proceeds in the so called reverse START-STOP mode, where detection starts a high granularity timer stopped by the next excitation pulse. The bin granularity ranges between a few and tens of picoseconds in time windows of tens of nanoseconds.. BS: beam splitter; ND: neutral density filters; CFD: constant-fraction discriminator; TAC: time-to-amplitude converter; ADC: analog-to-digital converter.

indicator, particularly in non-purified biological fluids or inside cells and tissues.

Although there exist several methods to measure the fluorescence lifetime of a dye, including frequency domain assessments [98,99] and analog fluorescence pulse temporal profiling through streak-cameras [100], TCSPC offers superior versatility and cost-effectiveness. Moreover, the need to work with pulsed excitation in the single photon regime intrinsically limits the average excitation intensity to the tens of

microwatts range and minimises thermal effects, so that photodamage is usually negligible even when tight focusing is pursued. The major limitation of this technique consists in the time needed to reconstruct an accurate decay distribution, which can be of several seconds or even minutes for short digitisation bins and long-lived fluorophores.

Optical tomography and optical biopsy techniques based on the analysis of the time-of-flight (TOF) distribution of NIR photons emerging (either transmitted or back-reflected) from living tissues are other exemplary applications of TCSPC [101–103]. These techniques rely on the observation that photons scattered several times travel for a longer time before being detected. Thus, picosecond long light pulses interacting with denser and/or thicker tissues emerge with a delayed and broadened temporal profile. This profile can be reconstructed by means of either TCSPC or streak-camera-based measurements, although scattered pulses are typically very dim and streak-camera detection practically results to be feasible only at irradiation intensities incompatible with clinical safety requirements. The reconstructed profile, the so-called TOF distribution, bears information of the density and composition of the irradiated tissue. Fitting of the TOF distribution allows extracting such information. A further implementation of TOF analysis consists in the discrimination of the early arriving, minimally deflected (snake) photons from the ones undergoing multiple scattering. This can be achieved by combining sharp temporal resolution with spatial mode selection. Early arriving photons are collinear with the impinging beam, while after being significantly deflected, a photon may only accidentally be aligned along the original direction. In the case of snake-photon based optical imaging, optical discontinuities within tissues can be detected and localised with sub-millimetre resolution, and their nature assessed non-invasively, by simply scanning the tissue and measuring point-by-point the snake-to-scattered photon ratio [104–106].

2.4. Imaging

Imaging, namely recording a map of the quantity of interest in the sample under test, is opening up new perspectives in biophotonics and it is yet today a domain where techniques are in the early development stage.

Fluorescence microscopy, i.e., the recording of images of fluorescently stained cells or tissues, either in vivo or ex-vivo, provides information on the intracellular/intra-tissue environment or composition, as well as on biochemical reactions. In its simplest version, fluorescence imaging is used to visualise specific structures within the sample, e.g. cytoplasmic organelles, using fluorochromes which specifically bind to them. The pH dependent emission of some dyes is also frequently used as a sub-micrometre resolved litmus test. Wide field fluorescence imaging can be performed with standard CCD cameras at high frame rates to monitor ion gradients in living tissues, e.g. calcium imaging in neuronal networks. However, this technique is endowed with poor spatial resolution since the whole sample is illuminated at once and fluorescence is isotropic.

An improvement is offered by confocal fluorescence microscopy [107–112], exploited to detect the fluorescence emitted by sub-micrometric spots within the sample. Moreover, it features optical sectioning, namely the selection of light produced only in the focal plane, with a depth defined at micrometre level. In its simplest embodiment, confocal microscopy is realised using a flying-spot technique, where the excitation laser beam, deflected by galvanometric mirrors, is scanning the sample and for every stop the fluorescence intensity is measured with a point-like detector, usually photodiodes or PMT. Typically, the step size is at the 100 nanometre scale and sample areas of 500 × 500 steps allow imaging a small number of cells in a few seconds, with dwell times of about 10 μs per pixel.

The integration of picosecond or even femtosecond pulsed laser sources and single-photon sensitive detectors within scanning beam microscopy systems in the early 1990's paved the way for multiphoton-excited fluorescence microscopy [113,114], a significant alternative to confocal geometry. Due to the negligible probability of out-of-focus fluorescence excitation, this technique is inherently endowed with sharp optical sectioning and achieves higher spatial resolutions than confocal microscopy. Moreover, out of focus photodamage is significantly reduced and depth of penetration within tissues increased. As a drawback, the low multi-photon absorption cross-section compels to use single-photon sensitive detectors even for routine intensity map reconstruction. Moreover, the requirement for rather expensive excitation sources limits the diffusion of this technique [115]. Confocal and multiphoton microscopy can be implemented using single-photon counting detectors and suitable staining procedures to obtain maps of the fluorophore concentration, brightness, and diffusion coefficient through pixel-by pixel Fluorescence Fluctuation Spectroscopy (FFS) [97]. Moreover, with the additional requirement of using pulsed excitation also in the confocal configuration, it is possible to obtain maps of the fluorescence decay time and even local fluorescence decay distributions, a technique which is referred to as Fluorescence Lifetime IMaging (FLIM) [97]. A common limit of these implementations is the long dwell time needed to acquire statistically significant information, exceeding hundreds of milliseconds per pixel for FLIM and tens of seconds for FFS. In order to overcome this shortcoming, in FLIM two different strategies were historically adopted. The use of CCD cameras coupled with time-gated image intensifiers in wide-field fluorescence microscopy set-ups allowed rather fast reconstruction of fluorescence decay maps at low spatial resolution with no optical sectioning, which nonetheless demonstrated to be favourable for certain applications [116,117]. Furthermore, the development of spatial light modulation technologies allows for multi-spot multiphoton excitation, opening new perspectives for parallelised fluorescence decay patterns recording highly resolved in space and time [118,119]

The last class of fluorescence-based imaging techniques which is worth recalling is super-resolution microscopy (Fig. 5), namely imaging below the diffraction limit down to tens of nanometres spatial resolution [121,122]. This technique is essentially based on two different approaches. On one hand, a patterned excitation of the sample is exploited in what is referred to as STimulated Emission Depletion microscopy (STED) and related methods. On the other hand, the image is built from the centre of gravity of diffraction limited localisation of stochastically excited individual fluorescent molecules in PhotoActivated Localisation Microscopy (PALM), STochastic Optical Reconstruction Microscopy (STORM), Super-resolution Optical Fluctuation Imaging (SOFI). These techniques require acquisition of multiple frames for the same specimen, with high sensitivity sCMOS and EMCCD cameras. A current limitation of super-resolution fluorescence microscopy techniques consists in the

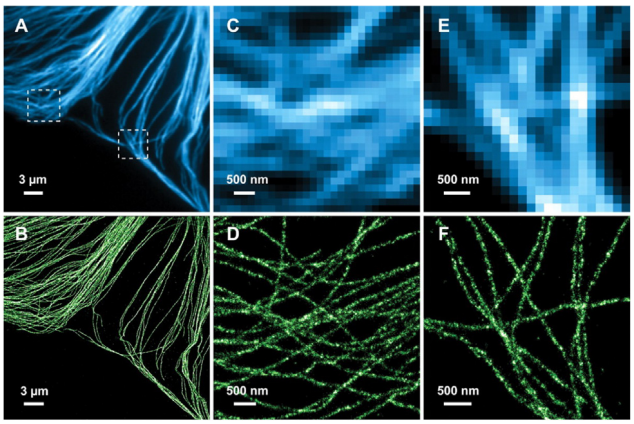

Fig. 5. Conventional confocal fluorescence microscopy (top row) and STORM super-resolution fluorescence microscopy images (bottom row) of microtubules within a cell. Panels A and B show wide field images; panels C, D and E, F correspond to the highlighted areas in panel A. The measured spatial resolution of the STORM images is 30 nm.
Source: Reproduced from [120].

relatively long acquisition time needed to obtain an image with respect to conventional fluorescence microscopy, trading off spatial resolution with speed. In patterned-excitation based methods, the loss of temporal resolution with respect to scanning-beam confocal microscopy is due to the need of reducing the pixel size according to the desired spatial resolution, while the dwell time cannot be pushed under a certain threshold dictated by the emission rate of the imaged fluorophore. Single-molecule localisation is limited by the probe switching kinetics, the camera acquisition rate and the required statistics [123].

3. Beyond the state-of-the-art: exemplary illustrations in the use of sipm for biophotonics

For each class of techniques outlined in the previous section, the published literature reporting applications of SiPM and SPAD imagers has been analysed. Exemplary illustrations have been selected to show the advances and the current limitations. The choice has not been based on the latest sensor architectural and technological advances, eventually addressed in Section 4, but on the readiness level of the specific application. A subsection has been dedicated to demonstrations of the potential of these sensors in association to micro-fluidic chips.

3.1. Intensity & counting

Two exemplary proofs of concept were designed and completed by a team at the University of Science and Technology in Krakow (Poland) which targeted both measurements of fluorescence in intensity mode [124] and chemiluminescence in counting mode [125].

As far as fluorescence is concerned, tests were performed with a solution of fluorescein in Tris Buffered Saline by Sigma-Aldrich, with concentrations spanning six orders of magnitude, with a lower value of 0.0027 pmol/ml. The solution was flowing in a microfluidic slide (μ-Slide by Ibidi GmbH, located in Munich, Germany; http://www.ibidi.com), with channels 5 cm long, 5 mm wide and 0.1 and 0.6 mm deep at a rate of 20 µl/min. Fluorescence was excited by a 60 mW laser (Phoxx by Omicron Laserage GmbH, Dudenhofen Germany; https://www.omicron-laser.de) pulsed at 100 kHz frequency, emitting at 488 nm with pulse duration in the 10–25 ns range. Light was conveyed to the slide by an optical fibre with a 5 mm diameter collimator. Scattered and stray excitation light was reduced protecting the SiPM with a filter (Biotek 530/30, http://www.biotek.com) with a 30 nm bandpass. Measurements were performed using a sensor by Sensl (model MicroFC-SMTPA-10035, 1 mm^2 area, 35 µm cell pitch). The sensor signal was readout synchronously to the laser excitation by a custom designed ASIC [126], based on a Charge Sensitive Amplifier followed by a Peak & Hold circuit. The intensity was measured by the mean value of the multi-photoelectron distribution collected over a large statistics. The trend of the peak value vs. the fluorescein concentration is shown in Fig. 6; as it can be seen by the empirical power law fit, the system response is not linear, possibly because of the onset of the saturation of sensor in use, characterised by a small number of pixels, or instabilities in the flow system. Nevertheless, the detector still retains a limited sensitivity, corresponding to a relative variation of the signal $(\Delta S/S) = 0.16 \times \Delta\rho/\rho$, being ρ the concentration of the fluorescein. The limit of detection is 0.0071 pmol/ml, for a signal three standard deviations away from the response for the pure buffer with no fluorescein.

Chemiluminescence by luminol was used [127] to investigate the possibility to measure the concentration of a spontaneous light emitting substance by counting. This technique is bounded by the fluctuations of the Dark Counts on the low end and by the event pile-up on the high end. Presuming the dark counts to be Poissonian distributed, the sensitivity increases with the squared root of the observation time, extremely depending on the specific phenomenon under investigation. The pile-up limit is depending on the time development of the signal, its shaping and possible digital processing in real-time. In the reported study, a fully differential circuit was designed, where the pre-amplifier

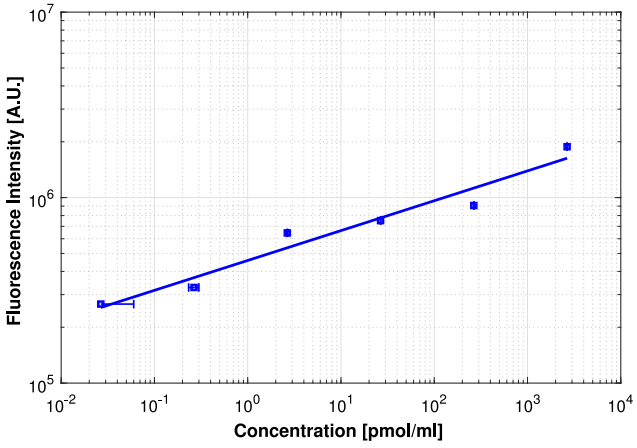

Fig. 6. Mean value of the detected light intensity (A.U.) in response to a variable concentration of fluorescein, spanning 6 orders of magnitude [126].

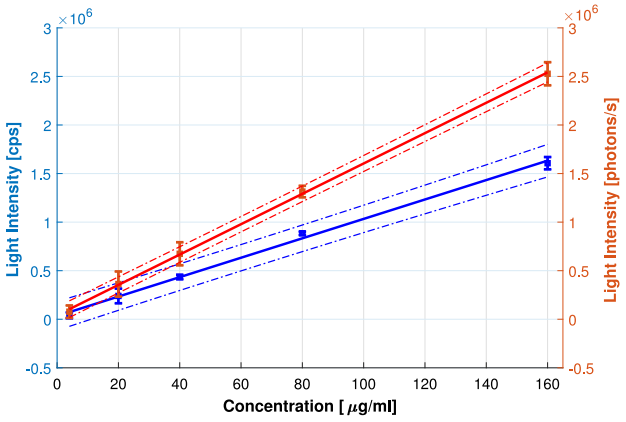

Fig. 7. Pulse frequency (in blue, scale to the left hand side) and average number of detected photons/s (red, scale to the right hand side) in response to a variable concentration of Luminol. Measurements were performed with time bins of 200 µs [127]. (For interpretation of the references to colour in this figure legend, the reader is referred to the web version of this article.)

was followed by a fast shaper based on a zero-pole cancellation tuned to comply with an HAMAMATSU MPPC S12571-100C sensor (1 mm^2 area, 100 µm cell pitch). The circuit provided single photo-electron pulses with a peaking time of 3.6 ns, a FWHM = 3.8 ns and a full signal development of about 10 ns, enabling counting with a pile-up probability not exceeding 5% up to 5 MHz mean frequency of a random Poissonian process. Experiments where performed with luminol concentrations up to 160 µg/ml in a 1 mol/l sodium hydroxide (NaOH) solution, with 30% hydrogen peroxide. The solution was hold in a cuvette and the SiPM was directly interfaced to the transparent wall. The sensor in use was characterised by a Dark Count Rate (DCR) of 100 kHz at room temperature and measurements were led in a time window of 200 µs. The response curve is shown in Fig. 7 corresponding to a sensitivity of 10^4 cps/(µg/ml) and a minimum detectable signal of 6.7 µg/ml, limited by the DCR and the short integration time. On the same figure, the second line shows a different approach where use is made of the fact that a single chemiluminescence emission corresponds to more than one detected photon. So, events may be weighted by their intensity to enhance the sensitivity. In this specific case, the light collection was not optimised and the net gain is limited. However, optimisation could lead to a significant improvement at least for this class of luminescence.

A set of tests on chemiluminescence detection with a SiPM based set-up in current integration and counting mode was performed by

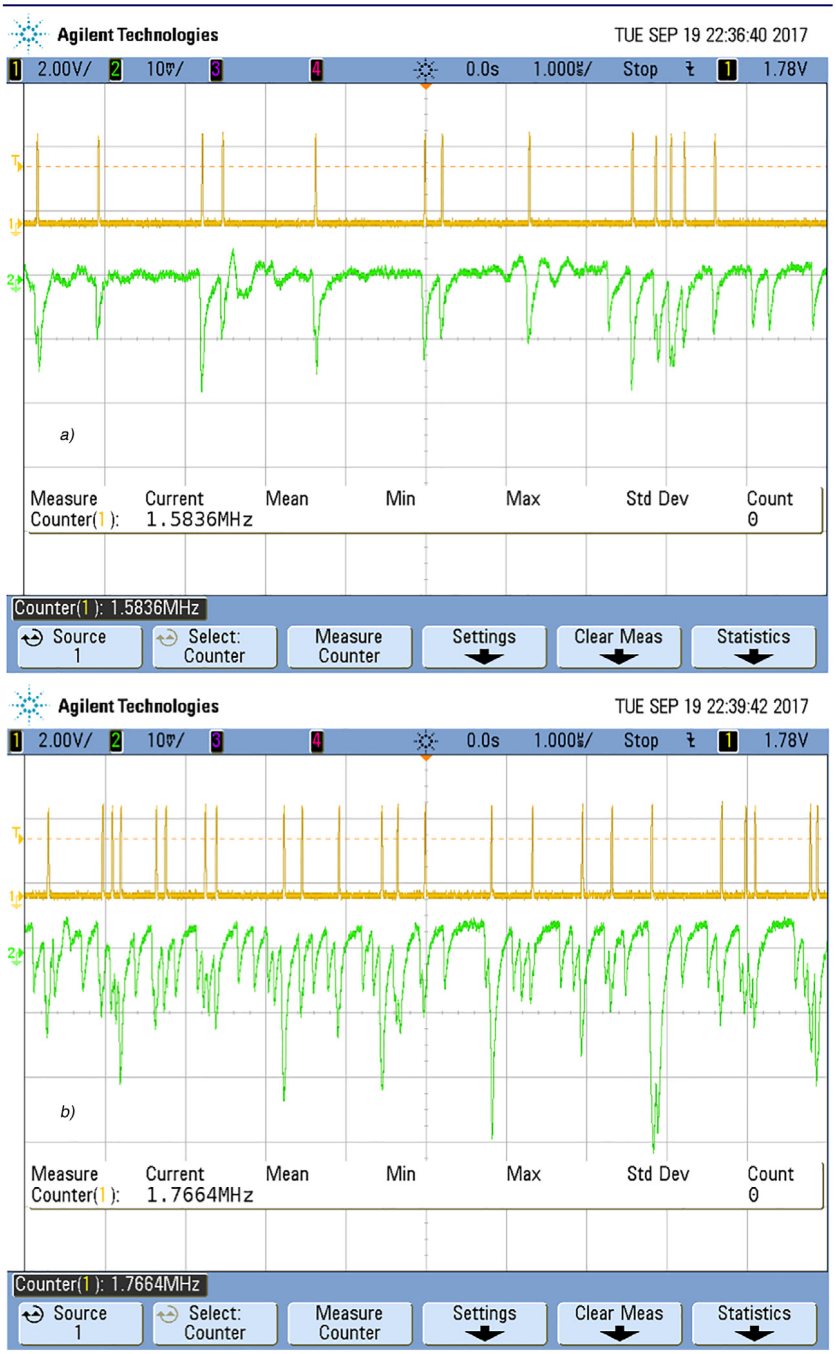

Fig. 8. Oscilloscope traces showing the chemiluminescence single photons emitted by cells in response to a stimulus. Panel a. corresponds to the injection of ATP, panel b. is related to TRITON, required to set the normalisation of the response. Signals refer to a nominal value of 1500 cells over a plate of 25 mm diameter.

three of the authors (M.C., R.S. and L.N.) together with a team from Universitá del Piemonte Orientale (Novara, Italy) lead by Dmitry Lim, a physiologist, and Carla Distasi, a biophysicist. The scientific background for the tests is the study of calcium signalling, essential in cellular physiopathology. The chemiluminescence probe in use is aequorin, a protein which, when activated in cell by coelenterazine, reacts with three Ca^{2+} ions to yield a single chemiluminescent photon. As a consequence, an external stimulus triggering intracellular Ca^{2+} release, such as administration of adenosine-triphosphate (ATP), induces an increase in chemiluminescence. Monitoring the temporal evolution of the chemiluminescence signal allows to reconstruct the shape of calcium spikes, which is frequently significant of diseases. In contrast with most assays based on Ca^{2+} sensitive fluorophores, the response in the aequorin assay is directly proportional to the Ca^{2+} intracellular concentration, which increases from the basal value of tens of nanomolars to fractions of micromolar when the stimulus is delivered. An additional advantage of aequorin is that external excitation is obviously not needed, thus preserving the cells from photodamage and making the measurements more robust with respect to systematics related to detection of excitation stray light. The experiment can be made quantitative as long as a normalisation of the ATP induced signal is provided. In our tests, this was achieved by a delayed disruption of all of the cells in the sample with a surfactant (TRITON X-100, available by different producers) to consume the residual amount of aequorin through reaction with extracellular Ca^{2+}, present at the concentration of 2 mM both in vivo and in pseudo-physiological buffers. In experimental terms, this is inducing a significant difficulty, since the normalisation signal is expected to exceed by nearly a factor 50 the ATP induced intensity, requiring a

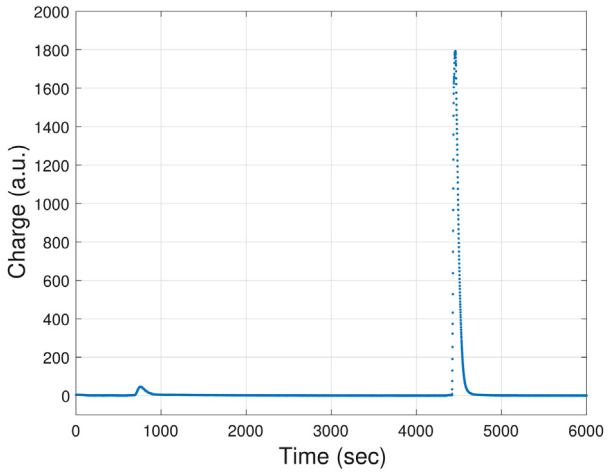

Fig. 9. Response of a cell sample to the ATP (low signal) and TRITON (high signal). The output of the SiPM in use was directly digitised by a QDC. The effective time bin corresponds to 5 ms. Signals correspond to a nominal number of 10^5 cells.

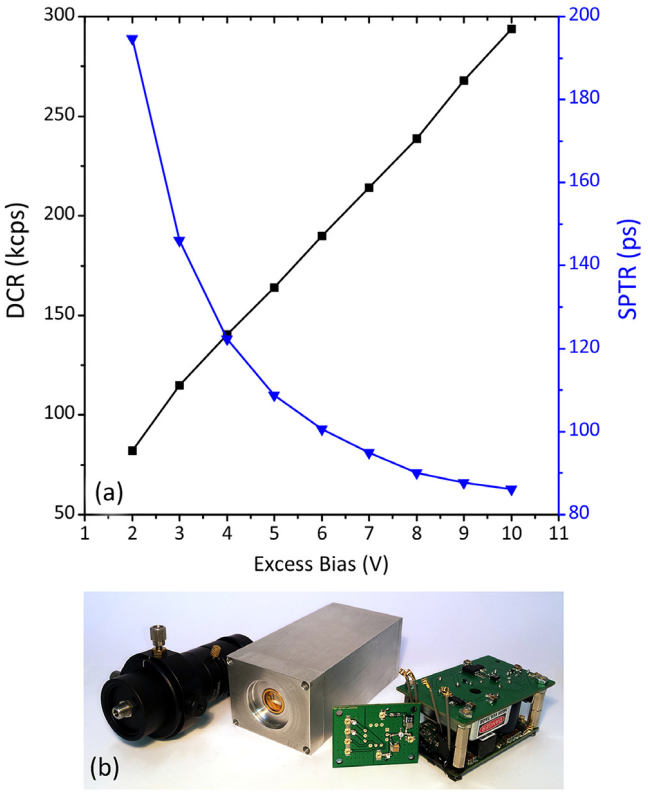

Fig. 10. (a) Dark count Rate and Single Photon Timing Resolution as a function of excess bias voltage (b) Picture of the module designed by Martinenghi et al. [128].

further extension of the dynamic range. Technology wise, the activity was motivated by the end-user request to develop an instrument that could replace a custom made PMT based apparatus, offering at least comparable performance with a lower cost, modularity, flexibility and, primarily, portability.

Experiments were performed in counting and integration mode using a HAMAMATSU S13360-6050CS sensor, with 6 × 6 mm^2 area, integrating 14400 cells with 50 μm pitch. The sensor, characterised by a DCR at the MHz level at room temperature, was biased through the CAEN SP5600 power supply and amplification unit. The signal was amplified by the same module and the count rate at 0.5 photo-electron discrimination level retained as a measurement of the intensity. The number of pulses was counted over a 5 ms time bin, with a three standard deviation minimum signal detection corresponding to a frequency increase of 42 kHz over the DCR. In integration mode, the signal from the sensor was directly fed into a CAEN V752N charge-to-digital converter (QDC). The integration time was 5 μs to cope with the QDC dynamic range and the signals were averaged over 1000 samples for a time bin equivalent to the counting procedure. The sensor was mounted in a dedicated holder and interfaced to a cell plate with diameter of 25 mm, through index matching optical grease. The range of interest in the number of cells/plate has a lower limit at 700 and an upper limit at 400 000, with a significant signal variation further scaled up by the corresponding intensity of the TRITON induced signal.

An exemplary illustration of the pulse density in time is shown in Fig. 8, for the ATP stimulus and after the injection of the surfactant. These exemplary oscilloscope screen shots correspond to a number of cells/plate equal to 1500, on the low end of the required range. It is evident that the measurement of the ATP induced signal is well possible even with no signal shaping. However, the surfactant is expected to induce pulsing frequencies up to 100 MHz at the highest number of cells, well beyond what the system can comply with, even shaping the signal to a full duration at the 10 ns level. The full time development of the signal in integration mode is shown in Fig. 9 for a number of cells equal to 10^5. The signals induced by both the ATP and the TRITON are clear and well reconstructed, with no indication of saturation. However, the sensitivity is limited and no ATP induced response was visible for a number of cells below 25 000.

3.2. Timing & imaging

3.2.1. Time correlated single photon counting

The two major challenges in TCSPC for the analysis of the fluorescence signal are the engineering of cost-effective field instrumentation (e.g. clinical diagnostics and food quality during harvesting) and the development of solutions to the limitations on the time stamped photon rate, impacting on the total duration of the measurement.

An exemplary illustration of the development of a compact system is reported by Martinenghi et al. [128], who designed and qualified a SiPM based module (Fig. 10) using a 1 mm^2 area sensor by Excelitas (model C30742-11-050-T1). The major advantages seen in this solution are the limited voltage and power consumption, enabling battery operation, the larger sensitive area with respect to SPAD, reducing the requests on the optics, and the fact that the SiPM is essentially dead-timeless for a low frequency of impinging single photons. Possible limitations are rather obviously connected to the DCR and the temperature dependence of the gain. The authors studied the DCR and the Single Photon Transit time Resolution (SPTR) dependence on the excess bias voltage (Fig. 10). Requiring a SPTR of 100 ps, a DCR of about 170 kcps was measured. This value was not considered to be a limiting factor. The temperature stability was achieved by thermo-electric cooling with the possibility to maintain the sensor at temperatures as low as −10 °C.

In standard TCSPC, the major limitation in the sustainable rate of detected photons is primarily resulting by the stochastic arrival of photons during the system dead-time (pile-up), due to the detector and the use of a single circuit for the stamping and digitisation of the time of arrival. The former can be as low as 30 ns level [130] for actively quenched SPAD while the latter can be as long as hundreds of nanosecond [131], de facto being the bottle neck. Pile-up significantly distorts the distribution of the time of arrival, biasing the measurement of the fluorescence lifetime towards lower levels. In order to minimise the effect, current systems operate at a rate of detected photons not exceeding 5% of the excitation rate. This limitation can be overcome by using SiPM, seen as a collection of individual SPAD, uniformly illuminated by the fluorescence light in order to scale down the firing probability/cell to a level where the impact of the recovery time of the single cell is negligible. This is shifting the problem to the signal

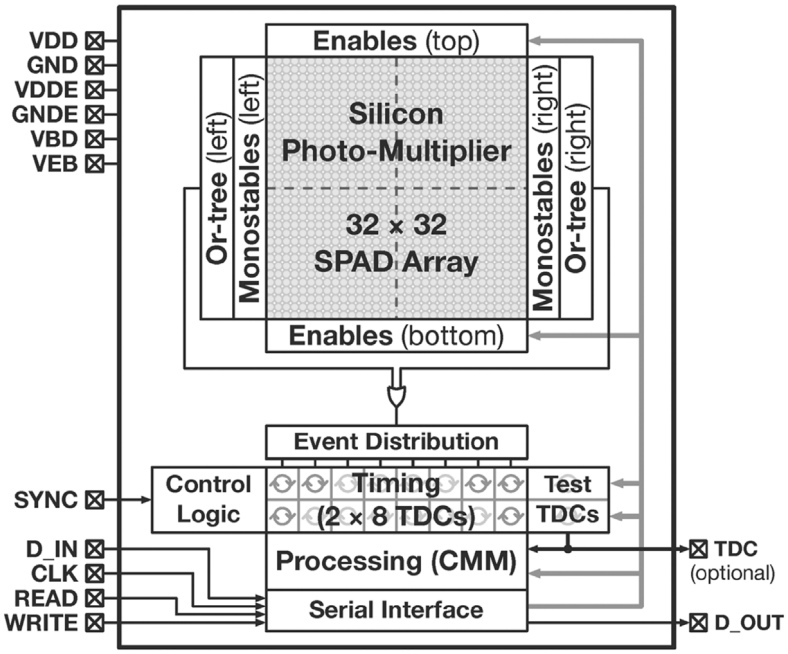

Fig. 11. Block diagram of the architecture implemented by Tyndall et al. [129].

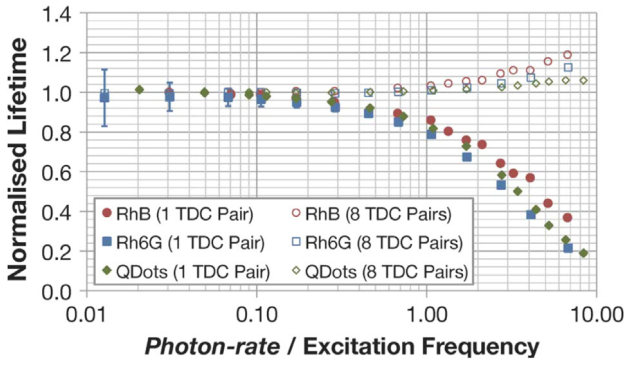

Fig. 12. Normalised lifetime for three different fluorophores with lifetimes ranging from 1.74 to 20 ns. The test is performed enabling and disabling the multiple TDCs chain at increasing photon rate per excitation frequency [129].

processing, in terms of identifying nearby signals by different cells, time stamping them and evacuating at high throughput the information. An exemplary architecture has been proposed by Tyndall et al. [129]. They designed an array of 32 × 32 SPAD in CMOS technology (Fig. 11) where the signal by each cell is connected to a pulse-shortening circuit producing a train of monostable signals ≈ 400 ps long.

The most relevant feature of the proposed architecture consists in the implementation of a multiple channel timing architecture based on 8 pairs of TDCs with 50 ps resolution, reducing the problem related to the digitisation of the times of arrival of the detected photons. TDC are organised in pairs, so that one TDC is active and available to accept an event while the other is outputting its data and being reset. The train of pulses is distributed to the battery of TDC pairs by a token-passing shift register.

To demonstrate the ability to overcome the pile-up effect, the normalised lifetimes measured with three types of fluorophores with expected lifetime of 1.74 ns, 4.08 ns and 15–20 ns have been measured at increasing photon rate, enabling and disabling the multiple channel timing architecture. The plot in Fig. 12 clearly shows the potentiality of this system, where even at this preliminary stage a gain in photon rate up to a factor 20 is possible. Moreover, it is worth remarking that the authors developed as well an algorithm for a real time calculation of the lifetime [133] implemented on an FPGA, significantly contributing to the reduction of the data throughput.

3.2.2. *Fluorescence lifetime imaging*

Indexing the cells of a SPAD array and embedding time stamping and advanced functionalities on pixel would represent a breakthrough in FLIM, so far limited by either the use of single-point PMT or SPAD based instruments or by the limited temporal sensitivity of cameras. A number of teams have been developing SPAD arrays in CMOS technology targeted to this application with significant advances in terms of:

- reducing the dark count rate from MHz to few tens of Hz per pixel [134];
- optimising the design, bringing the Photon Detection Probability (PDP), namely the product of the quantum efficiency and the avalanche triggering probability, from a few % to values close to 30% [135,136], for fill factors approaching 20% [137,138];
- implementing and comparing different timing solutions (TAC [139], TDC [140] or gating [141]);
- addressing the issue of data throughput and real-time processing, relevant as long as the dimension of the pixel matrix are scaled up [142,143];
- going beyond the pure sensor design and thinking in terms of system development.

An exemplary proof-of-concept of a full system (Fig. 13) based on a SPAD array is presented in [132], by Poland and co-authors.

The sensor consists in a 32 × 32 matrix with 50 μm pixel pitch and a photon sensitive area of 6 μm diameter. Every pixel (Fig. 14) integrates a 10-bit, low power TDC with 55 ps granularity, for a time range covering the needs for the majority of fluorophores. The FLIM set-up was designed engineering an array of 64 light beamlets, covering a field of view of 100 μm. Beamlets were generated starting from a 200 fs long pulse by a Ti:Sapphire Chameleon Ultra II laser, with 80 MHz repetition rate. The fluorescence light was focused on the sensor plane with an optics mating the beamlet pitch to the sensor pitch and focusing light to a spot of 1.8 μm FWHM centred on the sensitive area of every pixel. Data from an 8 × 8 pixel sensor sub-array were transferred to the equipment PC via USB, with a maximum throughput of 280 Mb/s. Data transmission was

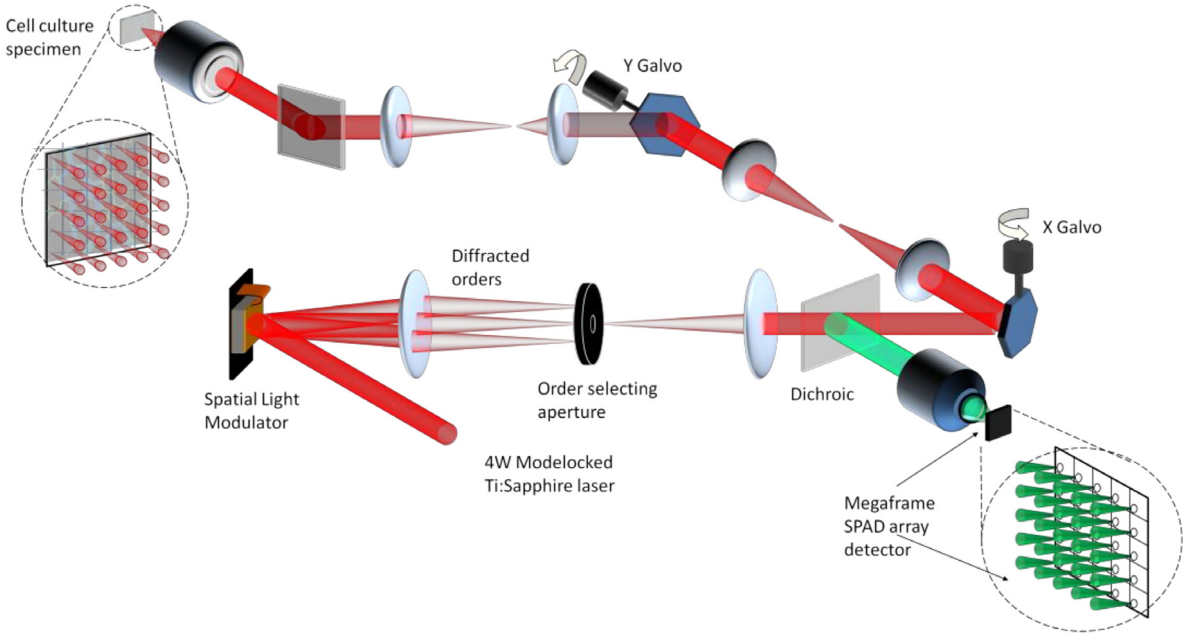

Fig. 13. Operational schematic of the multifocal multiphoton system used by Poland et al. [132].

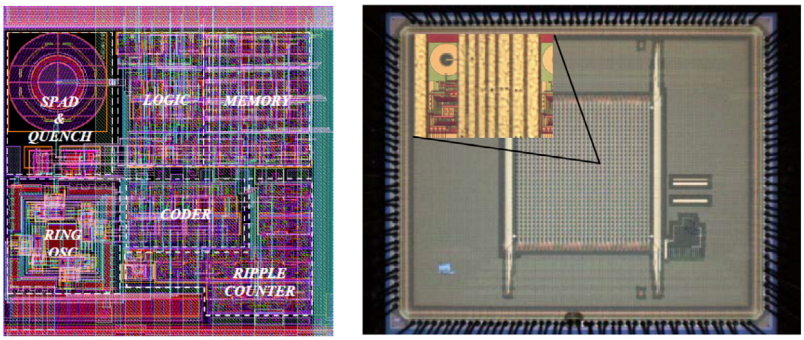

Fig. 14. Pixel layout of the Megaframe SPAD array (left) and 32 × 32 SPAD-TDC array Micrograph (right) [144].

actually a limiting factor, forcing to reduce the photon rate to provide 250×10^3 time stamps/pixel/s, half of the maximum rate sustainable by the sensor. Nevertheless, the system recorded images at a speed increased by a factor 20 with respect to a flying-spot, point-like sensor based set-up with a photon rate at the 1% level.

The 8 × 8 array was scanned over 32 × 32 positions, providing a series of 256 × 256 pixel images. Tests were performed imaging two steps involved in the signalling of receptor tyrosine kinases in live human breast carcinoma cells. In details, the interaction between the Epidermal Growth Factor Receptor (EGFR) family members HER2 and HER3 was considered, relevant in tumour genesis and treatment resistance in breast cancer. Exemplary illustrations of the image quality are shown in Fig. 15, together with a comparison between the fluorescence time resolution obtained with this system and with a time gated architecture, clearly showing advantages beyond the pure imaging acquisition time due to the parallel architecture.

3.2.3. Super-resolution microscopy

The power of indexing the elements of a matrix of single photon sensitive cells can also be illustrated by the results achieved in super-resolution microscopy, where the absence of excess and readout noise can be expected to lead to superior localisation precision. An exemplary illustration is reported in [145], based on the SwissSpad, an array of 512 × 128 SPAD pixels with 24 μm pitch. Beside a quenching circuit, every pixel integrates a 1-bit memory cell, recording the detection of a photon or the occurrence of a spurious avalanche. The readout is performed using a rolling shutter architecture with a 6.4 μs frame period. The integration of the on-pixel functionalities reduces the fill factor to 5%, partially compensated by micro-lensing leading to an effective fill factor of 60%, for a peak Photon Detection Efficiency of 20% at 450 nm. The median distribution of the Dark Count Rate per pixel is 200 cps at room temperature, with a significant difference with respect to the mean value due to about 2% of hot pixels. The SwissSpad was integrated into a super-resolution microscopy set-up based on Ground-state Depletion and SIngle-Molecule return (GDSIM) [146], with a lensing system featuring a magnification by a factor 160, for an effective pixel size 150 nm. The system was designed to host two detectors and the performance of the SPAD array was compared to a scientific CMOS (sCMOS) camera (model edge 4.2 by PCO, Kelheim, Germany; the camera features a peak QE of 82%) and to an Electron Multiplying CCD (model iXon3 897 BV by ANDOR Technologies, Belfast, UK; the camera is back illuminated and features a QE in excess of 95%). The quality of the recorded images is shown in Fig. 16, relative to GATTAquant PAINT 80 R nanorulers (http://www.gattaquant.com/products/localization-based/gatta-paint-nanoruler.html) where emitters are separated by 80 nm and the fluorescence light is red. The 6.4 μs 1-bit maps by the SwissSPAD were summed in 10 ms long frames, analysed by a dedicated software; the reported images correspond to the results of 5000 frames. The localisation uncertainty for the SwissSPAD was measured to be 20 nm, for 100 photons/frame. This has to be compared to 10 nm for the

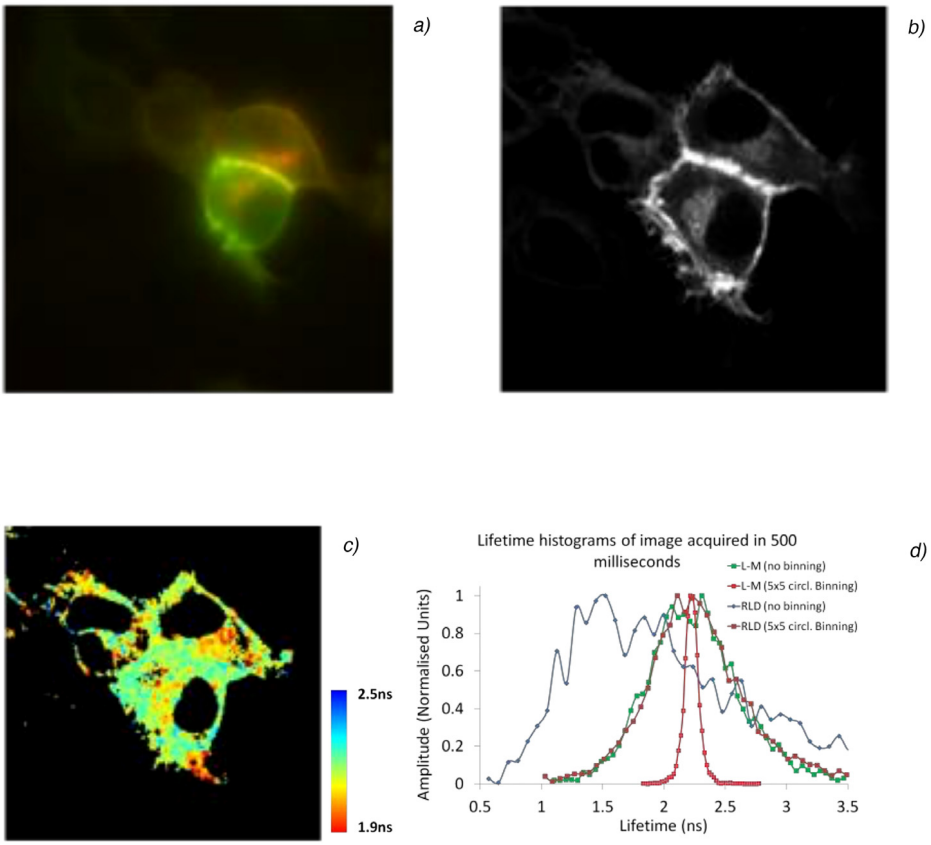

Fig. 15. Images of human breast-cancer cells acquired with different fluorescence microscopy techniques (adapted from [132]): (a) wide field fluorescence intensity map; (b) two-photon excited intensity map; (c) fluorescence lifetime map. In (d) the spread in the lifetime map obtained in (c) is compared to simulated time-gated data, to show that also the temporal resolution is superior in the case of the multi-beam set-up.

sCMOS, recording 800 photons/frame, and 15 nm for the EMCCD, recording 1800 photons but with a non negligible excess noise reducing the advantages due to the higher photon detection efficiency. The results obtained with the SPAD array are not yet competing with the top level available cameras neither in terms of spatial resolution, limited by the current photon detection efficiency, nor in terms of frame rate. In fact, the current readout frequency corresponds to 613 fps for an 8-bit image, while record streaming of up to 1600 fps were reported [147] in super-resolution imaging for the same number of pixels digitised at 16 bits, using an ORCA Flash 4.0 V2 sCMOS by HAMAMATSU Photonics. Moreover, hot pixels irreducibly induce a local image quality degradation.

The more critical point is possibly the PDE. In fact, as shown in the comparative analysis reported in [150], values at the 50% level are required to compete with state-of-the-art detectors in terms of spot identification capability. However, the availability of the high frequency 1-bit maps is certainly a unique asset. In fact, this has been proven [145] to provide the sensitivity to measure blinking of the fluorophores in the tens of microsecond range from the current ms values, essential for faster super-resolution procedures [147,151], the main development today.

3.3. Miniaturisation & parallelisation

The replacement of PMT tubes with SiPM offers the possibility to re-engineer existing systems, scaling down dimensions and costs and enabling parallelism, eventually leading to instruments with a broader application field. Relevant examples are offered by flow cytometry, where the collaboration between research teams and industry lead to systems either at advanced prototype or product level.

Techshot,[1] together with researchers from Purdue University, targeted the development of a micro-fluidic flow cytometer for point-of-care blood analysis [148,149].

The conceptual design of the system and the schematics of the disposable micro-fluidic chip are shown in Fig. 17 while a picture of the prototype, having dimensions of $8 \times 16 \times 18$ cm^3 is displayed in Fig. 18. In essence, a blood droplet taken from a finger prick is deposited on the microfluidic chip, realised in Polydimethylsiloxane (PDMS). The blood is mixed with fluorescent and magnetic labels. White Blood Cells (WBC) undergo dual labelling with magnetic beads (CD45 BioMag by Bangs Lab, Fishers, IN, U.S.A.) and fluorescence tags. Next the blood is pushed through the channels with a micro syringe. The WBC, present at a ratio 1:1000 with respect to Red Blood Cells (RBC), are magnetically separated towards the analysis channel and the RBCs continue down the main channel and then passively sorted into a branched channel for counting. The WBCs are illuminated with a LED source and in four detection stations the total count of WBC is performed, together with the measurement of Neutrophils, B-cells and T-cells. Fluorescence light is detected by SiPM (SPM-Micro with 1 mm^2 area and 100 cells, produced by Sensl). RBC count is performed by forward scattering and, due to the signal intensity, the sensor in use is a photodiode. The relevant dimensions of the microfluidic chip are reported in Fig. 19, engineered to have a flow in the main inlet channel of 10 μl/min, diverting 10% of the blood volume in the WBC channel and 10% of the volume in the RBC count channel, to keep the rate at sustainable level. The performance of the chip, magnetic sorting and count rates were validated by analysing the same test samples with a standard flow cytometer. In terms of signal processing, it is worth mentioning that a significant signal over noise enhancement was obtained pulsing the excitation LED at 100 kHz

[1] Techshot, Inc. Greenville, Indiana, USA; http://www.techshot.com.

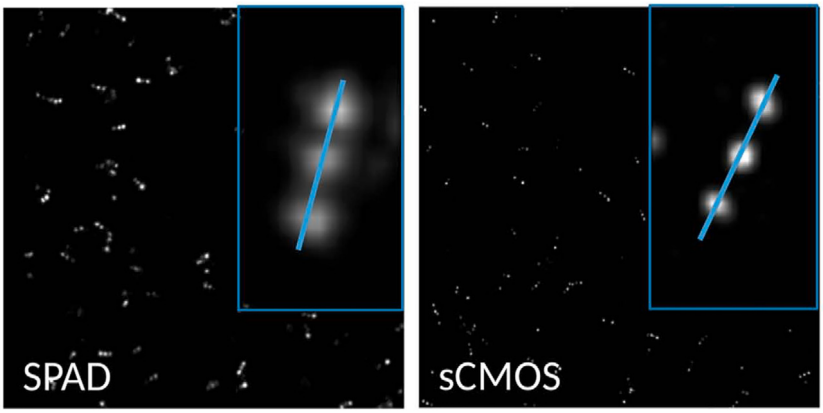

Fig. 16. Images of GATTAquant PAINT 80 R nanorulers, with emitters separated by 80 nm. The left-hand side panel shows the image obtained with the SwissSPAD, the right-hand side panel the image obtained with a sCMOS [145].

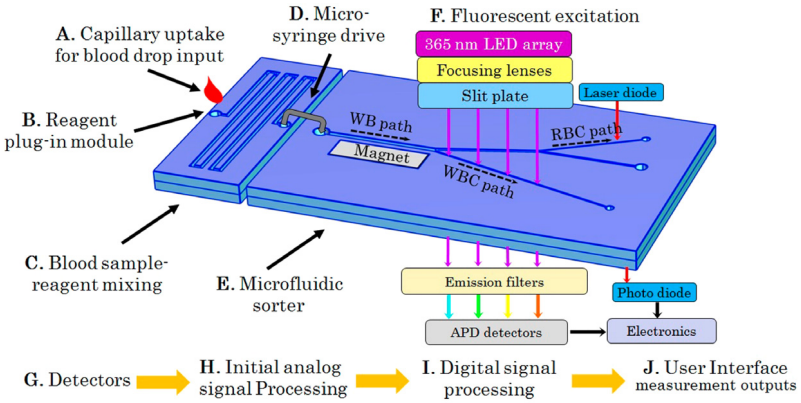

Fig. 17. Schematic of the micro-fluidic chip at the base of the cytometer designed by Techshot for point-of-care blood analysis [148,149].

frequency and using a lock-in amplifier in combination with a fourth-order low-pass filter.

Rqmicro,[2] a spin-off company of ETH-Zürich, is developing separation and detection technologies for microbiological tests in water and food. In particular, they designed and engineered a SiPM based complete system, possibly representing the first product on this market segment based on this class of sensors. Their cartridge-based liquid handling system completely separates the sample from the inner components of the instrument, eliminating the possibility for cross-contamination between samples. The entire optical system of their flow cytometer fits inside a small volume (3.5" high, 2 –1/8" wide, 7/8" thick), which is coupled to a motorised linear stage for automated alignment between the detection channel, being equivalent to the flow cell inside a traditional flow cytometer, and the optics. This enables the instrument to be moved to the point-of-use, where environmental samples are collected, without fear of misaligned optics or contamination of the fluid handling system. Such samples show large fluctuation in cell-to-cell signal intensity, even within the same population, requiring a high dynamic range sensor. For instance, the infectious bacterium Legionella pneumophila can have varying morphology depending on its environment, affecting the signal strength. Moreover, the measurement is affected by false-positive events resulting by non-specific binding of the fluorescent markers to particles and cell fragments in the sample. Biologists often require this background signal to be visible in their data as it is used as a reference against the signal of interest, typically a cell population with a specific fluorescent tag. An exemplary illustration of the detection signal by

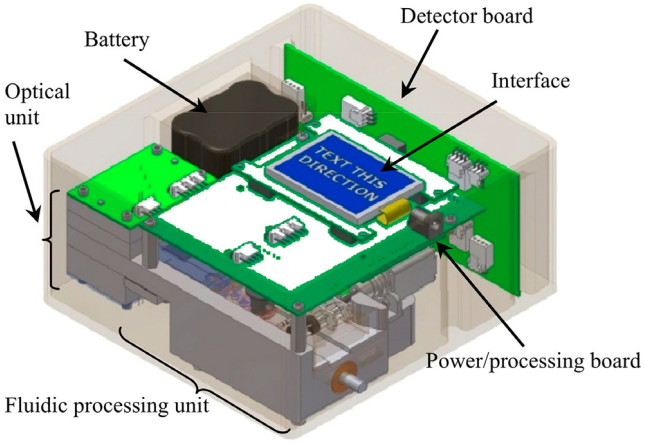

Fig. 18. Engineering view of the different components of the micro-cytometer [149].

labelled Legionella pneumophila bacteria in drinking water is shown in Fig. 20.

4. The way forward

Silicon Photomultipliers and SPAD imagers certainly have an enormous potential in biophotonics, especially when enhanced functionalities are integrated on chip. They can overcome some of the main limitations of the current techniques and bring to the development of

[2] Rqmicro AG, Brandstrasse 24, 8952 Schlieren, Switzerland; http://www.rqmicro.com.

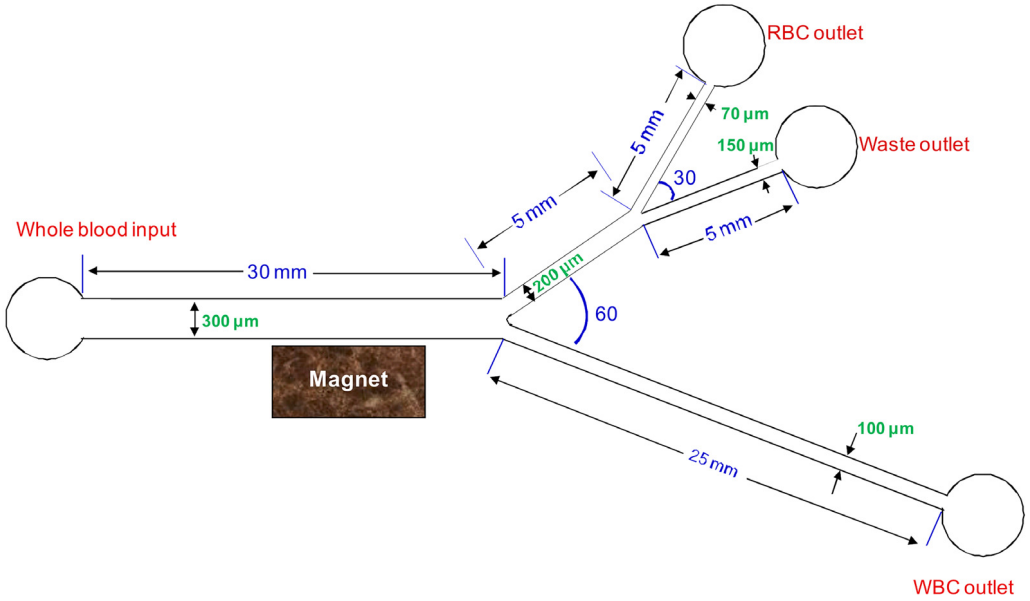

Fig. 19. Mask design for the microfluidic chip, showing the dimensions of the main inlet channel, the white cell and blood cell channels [148].

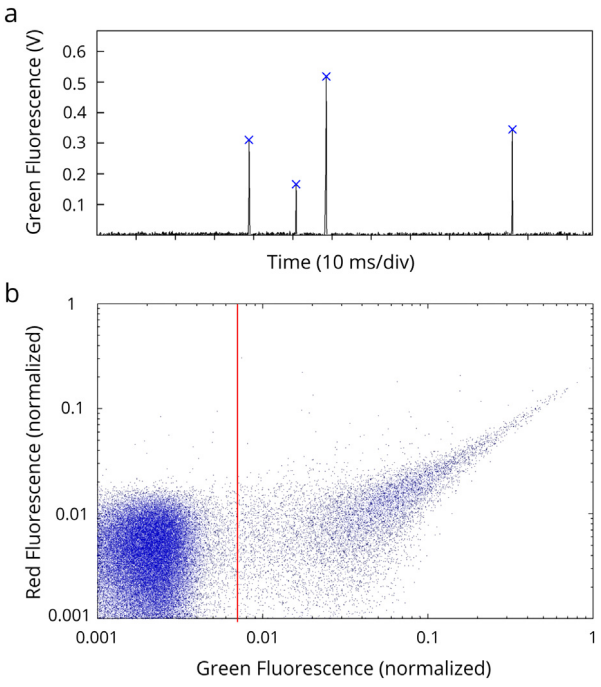

Fig. 20. Analysis of tap water spiked with Legionella pneumophila using rqmicro's portable flow cytometer. Panel a. shows the time-dependent green fluorescence signal recorded using an SiPM biased for a gain of 1.25×10^6 and a signal amplification by a factor 20. The peaks correspond to single cells passing through the interrogation point. Blue crosses mark the peak amplitudes used for quantification of the event. Panel b. is a scatter plot showing the fluorescence signal in the green channel (horizontal axis) and red channel (vertical axis). The Legionella pneumophila signal, to the right hand side of the red line, can clearly be discriminated against the background. (For interpretation of the references to colour in this figure legend, the reader is referred to the web version of this article.)

breakthrough methods. However, as outlined in the exemplary illustrations reported above and summarised in Table 1, their exploitation is currently limited by the sensor features and by system and engineering aspects so far unmet.

In terms of techniques based on the intensity of the signal associated to a constant illumination or resulting by long bio/chemi-luminescence, the request of covering typically 5–6 orders of magnitude makes the exercise not trivial. As long as the observable is the rate of detected single photons, the weakest signal of biological interest shall correspond to an increase in counting frequency given by $\nu_{min} = 3 \times \sqrt{\nu_{DCR}/\Delta t}$., where ν_{DCR} is the Dark Count Rate, Δt is the granularity of the time bin and a limit corresponding to three standard deviations of the noise floor fluctuations was assumed. Presuming $\Delta t \approx 100$ ms to probe the dynamics of the phenomenon and $\nu_{DCR} \approx 50$ kHz/mm^2, corresponding to the state-of-the-art figures at room temperature, then $\nu_{min} \approx 2$ kHz/mm^2. Scaling this value up by 5–6 orders of magnitude leads to a situation where the majority of the signals are piled-up, irrespective from any reasonable shaping. As a consequence, unless filtering of the light is assumed for the highest signals or the DCR is reduced by at least two orders of magnitude, the event rate technique has a limited applicability. However, a rather natural and obvious technique to cover the high-end of the required range consists in reading-out the SiPM in current mode or gated integration, where values up to hundreds of µA can be expected.

For fluorescence techniques based on pulsed light, the irreducible limitation in range and linearity comes by the density of cells in SiPM, with the highest reported number corresponding to 40 000 cells/mm^2 [156] and new concepts are being proposed [157]. As a consequence, systems must be engineered either optically spreading the light over large area sensors or reducing the system sensitivity or, once more, filtering the light in a controlled way.

Moving to SPAD imagers and, in general, SPAD arrays with integrated functionalities, the state-of-the-art is already extremely advanced and the recent results on the dark count rate/pixel highly significant. However, the Photon Detection Efficiency (PDE) is still today quite low and it limits their use. The use of micro-lensing [158] certainly represents a major progress but the breakthrough is represented by the recently reported activity on the vertical integration of sensors with VLSI electronics [159–161]. As already outlined in the previous section, as long as the PDE achieves 40%, this class of sensors is bound to become the reference for super-resolution microscopy [150] based on fluorophores with fast blinking. For TCSPC and FLIM, the reported results can already be considered one step beyond a proof-of-concept and the development of new architectures is very rapid. A significant example is reported in [162], where the chip hosting a 32 × 32 SPAD arrays integrates as well the circuitry for building 264 bins × 16 bit histograms of the time of arrivals of the detected photons. Histograms are evacuated from the chip at a maximal 188 kHz rate, enabling fast time resolved scanning. It is also worth mentioning line arrays of

Table 1
Summary table of the main biophotonic techniques, the sensors currently in use and their limitations. References to exemplary use of SiPM and SPAD imagers are also reported, outlining advantages and current limitations.

Application	Key figure	Sensors in use	Main limitations	SiPM / SPAD arrays: exemplary proofs of concept	Potential advantages & current limitations
Light Intensity Measurement					
Low throughput in vitro absorption and fluorescence / chemiluminescence analyses	Dynamic range (up to 6 orders of magnitude)	PMT (current mode), APD, Photodiodes	Sensitivity and limit of detection (fluorescence & chemiluminescence)	[126,127], aequorin assay reported in section 3.1	• Advantage: robustness and portability • Limitations: DCR on the low-end side and saturation on the high-end side
High throughput in vitro absorption and fluorescence / chemiluminescence analyses	Dynamic range (up to 6 orders of magnitude)	PMT, APD, Photodiodes	Acquisition time	None	• Advantages: parallel reading of a plurality of wells, miniaturisation • Limitations: DCR on the low-end side and saturation on the high-end side
Flow Cytometry / Cell sorting	Dynamic Range and separation in cell transit time at the μs level	PMT, APD	Miniaturisation, especially in view of point-of-care use	[149], Rqmicro in section 3.3	• Advantage: miniaturisation • Limitation: dynamic range
Photon counting techniques					
Fluorescence Correlation Spectroscopy / Photon Counting Histogram / Single Molecule FRET	Single Photon sensitivity and DCR versus signal count rate not exceeding 1%	PMT, SPAD	Poor (PMT)/no (SPAD) photon number resolution, long acquisition time, limited time granularity (pile-up driven)	[152]	• Advantage: photon number resolving capability (FCS, PCH) • Limitation: DCR
Functional Near IR Spectroscopy	Single Photon sensitivity, DCR versus signal count rate not exceeding 1%	PMT	Complexity and the need of HV	[153]	• Advantage: complexity reduction • Limitation: NIR sensitivity
Time Correlated Single Photon Counting	Single photon sensitivity and time resolution not exceeding 100 ps	PMT, SPAD	Photon rate not exceeding 5% of the excitation frequency	[128,129,154,155]	• Advantage: higher photon rate, multi-TDC architecture, on-chip histogramming, parallelisation for indexed SPAD arrays • Limitation: data throughput
Imaging					
Confocal fluorescence microscopy	Dynamic range, pixelised area (in the spinning disc architecture)	PMT (flying spot), EM-CCD (spinning disc)	Frame rate	None	• Limitation: hard to compete with sCMOS in terms of frame rate
Fluorescence Lifetime Imaging	Single photon sensitivity and time resolution not exceeding 100 ps	PMT, SPAD	Frame rate (flying spot technique)	[132,143]	• Advantage: higher photon rate, multi-TDC architecture; parallelisation for indexed SPAD arrays • Limitation: data throughput
Super Resolution Microscopy	Single photon sensitivity, pixelised area	EM-CCD, sCMOS	Frame rate and Excess noise	[145]	• Advantage: capability to resolve faster photo-switches • Limitation: PDE, frame rate

SPAD (see for instance [163]), enabling spectrally resolved fluorescence lifetime imaging [164–166] and FRET.

Concerning applications, SiPM are certainly the platform for miniaturisation and parallelisation. The reported illustrations linked to flow cytometry are exemplary and parallel reading of multi-well plates is, according to the authors, a technique where SiPM could boost an enormous progress also because of the possibility to reduce the quantity of biological material in use. NIR spectroscopy [6,96] is another technique where SiPM based miniaturisation is bound to play a role, as long as the spectral response is enhanced in the region of interest. An exploratory evaluation has been reported in [153] but unfortunately not pursued any further to our knowledge. Last but not least, it is worth mentioning the relevance of Fluorescence Correlation Spectroscopy and Photon Counting Histogram, possibly the only methods where the photon number resolving capability of SiPM can really represent a breakthrough. An early attempt has been reported in [152]. At the time, results were limited by the DCR and the optical cross talk, together with the extreme repetition rate of the laser in use. Today, with the continuous progress of the SiPM figures, also these techniques can be at hand.

Acknowledgements

The authors benefitted from discussions with several experts in the field and authors of referred publications. Among them, it is certainly worth acknowledging Giacomo Vacca at Kinetic River Corp., John Murphy at Sensl, Marco Mayer at HAMAMATSU, Wojtek Kucewicz, Piotr Dorosz and Mateusz Baszczyk at AGH-Krakow, Michel Antolovic at TU-Delft and Edoardo Charbon at EPFL-Lausanne. We also want to thank our co-workers on the reported early results on calcium signalling: Carla Distasi and Dmitry Lim at Universitá del Piemonte Orientale, Novara, Italy; Alexander Martemiyanov at ITEP-Moscow and Universitá dell'Insubria and Samuela Lomazzi at Universitá dell'Insubria.

References

[1] O. Shimomura, Bioluminescence: Chemical Principles and Methods, World Scientific Publishing Co. Pvt. Ltd, Singapore, 2006.
[2] A.K. Campbell, Chemiluminescence. Principles and Applications in Biology and Medicine, in: Ellis Horwood Health Science Series, Chichester, 1988.
[3] O. Hamdy, J. El-Azab, N.H. Solouma, M. Fathy, T.A. Al-Saeed, IEEE proceedings of the 8th Cairo International Biomedical Engineering Conference (CIBEC), Cairo, 2016, pp. 98–101.
[4] M.S. Wrobel, A.P. Popov, A.V. Bykov, M. Kinnunen, M. Jedrzejewska-Szczerska, V.V. Tuchin, J. Biomed. Opt. 20 (2015) 045004.
[5] W.D. Wilson, I.G. Lopp, Biopolymers 18 (1979) 3025.
[6] D. Contini, A. Torricelli, A. Pifferi, L. Spinelli, F. Paglia, R. Cubeddu, Opt. Express 14 (2006) 5418.
[7] W.F. Cheong, S.A. Prahl, A.J. Welch, IEEE J. Quant. Electr. 26 (1990) 2166.
[8] R.A. Stepnoski, A. Laporta, F. Raccuia-Behling, G.E. Blonder, R.E. Slusher, D. Kleinfeld, Proc. Natl. Acad. Sci. USA 88 (1991) 9382.
[9] V. Backman, R. Gurjar, K. Badizadegan, I. Itzkan, R.R. Dasari, L.T. Perelman, M.S. Feld, IEEE J. Sel. Top. Quantum Electron. 5 (1999) 1019.
[10] A. Lomakin, D.S. Chung, G.B. Benedek, D.A. Kirschner, D.B. Teplow, Proc. Natl. Acad. Sci. USA 93 (1996) 1125.
[11] J. Stetefeld, S.A. McKenna, T.R. Patel, Biophys. Rev. 8 (2016) 409.
[12] M. Hof, R. Hutterer, V. Fidler (Eds.), Fluorescence Spectroscopy in Biology. Advanced Methods and their Applications to Membranes, Proteins, DNA, and Cells, Springer-Verlag, Berlin, 2005.
[13] S.G. Schulman, Fluorescence and Phosphorescence Spectroscopy: Physicochemical Principles and Practice, Pergamon Press, Oxford, 2017.
[14] I.J. Joye, A. Draganski, J.A. Delcour, R.D. Ludescher, Food Biophys. 7 (2012) 138.
[15] A. Jimenez-Banzo, X. Ragas, P. Kapusta, S. Nonell, Photochem. Photobiol. Sci. 7 (2008) 993.
[16] L. Nardo, R. Paderno, A. Andreoni, M. Masson, T. Haukvik, H.H. Tonnesen, Spectrosc.: Biomed. Appl. 22 (2008) 187.
[17] M. Lilletvedt, H.H. Tnnesen, A. Hgset, L. Nardo, S. Kristensen, Pharmazie 65 (2010) 588.
[18] F. Cliquet, M. Aubert, L. Sagn, J. Immunol. Methods 212 (1998) 79.
[19] B. Herzog, H. Lemmer, H. Horn, E. Muller, BMC Res. Notes 7 (2014) 101.
[20] J.R. Blattner, L. He, J.J. Lemasters, Anal. Biochem. 295 (2001) 220.
[21] A. Holt, M.M. Palcic, Nat. Protoc. 1 (2006) 2498.
[22] D. Ni, P. Xu, S. Gallagher, Curr. Prot. Protein Sci. 88 (2017) 10.10.1.
[23] A.G. Gehring, D.M. Albin, S.A. Reed, S.-I. Tu, J.D. Brewster, Anal. Bioanal. Chem. 391 (2008) 497.
[24] A. Sassolas, B.D. Leca-Bouvier, L.J. Blum, Chem. Rev. 108 (2008) 109.
[25] M.J. Heller, Annu. Rev. Biomed. Eng. 4 (2002) 129.
[26] R.B. Stoughton, Annu. Rev. Biochem. 74 (2005) 53.
[27] S. Mancini, L. Nardo, M. Gregori, I. Ribeiro, F. Mantegazza, C. Delerue-Matos, M. Masserini, C. Grosso, Phytomedicine 42 (2018) 233.
[28] C.N. Pace, F. Vajdos, L. Fee, G. Grimsley, T. Gray, Protein Sci. 4 (1995) 2411.
[29] C.R. Cantor, P.R. Shimmel, Biophysical Chemistry, Vol. 2, W.H. Freeman and Co., S. Francisco, 1980.
[30] B.D. Wagner, Molecules 14 (2009) 210.
[31] O. Griesbeck, G.S. Bairs, R.E. Campbell, D.A. Zacharias, R.Y. Tsien, J. Biol. Chem. 276 (2001) 29188.
[32] A.D. Frankel, D.S. Bredt, C.O. Pabo, Science 240 (1988) 70.
[33] U. Cogan, M. Kopelman, S. Mokady, M. Shinitzky, Eur. J. Biochem. 65 (1976) 71.
[34] T.C. Jenkins, Optical absorbance and fluorescence techniques for measuring DNA-drug interactions. In: K.R. Fox (Ed.) Drug-DNA Interaction Protocols. Methods in Molecular Biology, Vol. 90, Humana press, Tonowa.
[35] A. Hillisch, M. Lorenz, S. Diekmann, Curr. Opin. Struct. Biol. 11 (2001) 201.
[36] K. Okamoto, Y. Sako, Curr. Opin. Struct. Biol. 46 (2017) 16.
[37] E. Sisamakis, A. Valeri, S. Kalinin, P.J. Rothwell, C.A.M. Seidel, Methods Enzymol. 475 (2010) 45.
[38] D.J. Wigelsworth, B.A. Krantz, K.A. Christensen, D.B. Lacy, S.J. Juris, R.J. Collier, J. Biol. Chem. 279 (2004) 23349.
[39] S.A. Sundberg, Curr. Opin. Biotech. 11 (2000) 47.
[40] L.M. Mayr, D. Bojanic, Curr. Opin. Pharmacol. 9 (2009) 580.
[41] R. Macarron, M.N. Banks, D. Bojanic, D.J. Burns, D.A. Cirovic, T. Garyantes, D.V.S. Green, R.P. Hertzberg, W.P. Janzen, J.W. Paslay, U. Schopfer, G.S. Sittampalam, Nature Rev. 10 (2011) 188.
[42] W.P. Janzen, Chem. Biol. Rev. 21 (2014) 1162.
[43] M.G. Acker, D.S. Auld, Perspect. Sci. 1 (2014) 56.
[44] E. Engvall, P. Perlmann, Immunochem. 8 (1971) 871.
[45] B. Berg, B. Cortazar, D. Tseng, H. Ozkan, S. Feng, Q. Wei, R. Yan-Lok Chan, J. Burbano, Q. Farooqui, M. Lewinski, D. Di Carlo. O.B. Garner, A. Ozcan, ACS Nano 9 (2015) 7857.
[46] S.Y. Toh, M. Citartan, S.C.B. Gopinath, T.-H. Tang, Biosens. Bioelectron. 64 (2015) 392.
[47] R.K. Saiki, S. Scharf, F. Faloona, K. Mullis, G.T. Horn, H.A. Erlich, N. Arnheim, Science 230 (1985) 1350.
[48] E. Le Poul, S. Hisada, Y. Mizuguchi, V.J. Dupriez, E. Burgeon, M. Detheux, J. Biomol. Screening 7 (2002) 57.
[49] B.W. Nieuwenhuijsen, Y. Huang, Y. Wang, F. Ramirez, G. Kalgaonkar, K.H. Young, J. Biomol. Screening 8 (2003) 676.
[50] D.W. Ow, J.R. De Wet, D.R. Helinski, S.H. Howell, K.V. Wood, M. Deluca, Science 234 (1986) 856.
[51] Z.M. Kaskova, A.S. Tsarkova, I.V. Yampolsky, Chem. Soc. Rev. 45 (2016) 6048.
[52] O. Shimomura, F.H. Johnson, Y. Saiga, J. Cell Comp. Physiol. 59 (1962) 223.
[53] S.E. Webb, E. Karplus, A.L. Miller, Mol. Reprod. Dev. 82 (2015) 563.
[54] https://www.biotek.com/resources/technical-notes/the-select-series-96-/384-well-microplate-reader-and-washer-for-hts-and-drug-discovery/.
[55] A. Adan, G. Alizada, Y. Kiraz, Y. Baran, A. Nalbant, Crit. Rev. Biotech. 37 (2016) 163.
[56] F. Traganos, Cancer Investig. 2 (2009) 149.
[57] M.J. Wilkinson, Trends Food Sci. Technol. 78 (2018) 1.
[58] J. Vives-Rego, P. Lebaron, G. Nebe-von Caron, FEMS Microbiol. Rev. 24 (2000) 429.
[59] A. Alvarez-Barrientos, J. Arroyo, R. Canton, C. Nombela, M. Sanchez-Perez, Clin. Microbiol. Rev. 13 (2000) 167.
[60] H.M. Davey, D.B. Kell, Microbiol. Mol. Biol. Rev. 60 (1996) 641.
[61] Z. Shutao, et al., High gain avalanche photodiode (apd) arrays in flow cytometer optical system, in: International Conference on Multimedia Technology, 2011.
[62] J. Tung, et al., CytoFLEX System Performance Evaluation, CYTO2015, Wiley, Liss, Glasgow, 2015.
[63] https://www.beckman.com/coulter-flow-cytometers/cytoflex/s-model.
[64] G. Vacca, K.P. Shevgaonkar, N.V. Hawk, V. Kapoor, W. Telford, A modular platform for flexible flow cytometry, in: XXXII International Congress of the International Society for Advancement of Cytometry, Boston, MA, 2017.
[65] H.M. Shaprio, et al., Practical Flow Cytometry, fourth ed., John Wiley and Sons, New Jersey, 2003.
[66] W.A. Bonner, H.R. Hulett, R.G. Sweet, L.A. Herzenberg, Rev. Sci. Instrum. 43 (1972) 404.
[67] L.A. Herzenberg, D. Parks, B. Sahaf, O. Perez, M. Roederer, L.A. Herzenberg, Clin. Chem. 48 (2002) 1819.
[68] https://www.semrock.com/flow-cytometry.aspx.
[69] J.R. Lakowicz, K.W. Berndt, R.A. Hoffman, B.G. Pinsky, US patent - US5504337A, 1996.
[70] W. Li, K.D. Houston, J.P. Houston, Sci. Rep. 7 (2017) 40341.
[71] G. Vacca, K.P. Shevgaonkar, R. Jimenez, A. Singhal, D.G. Vacca, D.J. Schodin, R.R. McKay, More robust fluorescence lifetime measurements for cell biology and multiplexing, in: XXXIII International Congress of the International Society for Advancement of Cytometry, Prague, Czechia, 2018.
[72] G. Vacca, K.P. Shevgaonkar, R. Jimenez, D.G. Vacca, A. Singhal, R.R. McKay, D.J. Schodin, Compensation-free flow cytometry based on fluorescence lifetime, in: XXXIII International Congress of the International Society for Advancement of Cytometry, Prague, Czechia, 2018.
[73] S. Weiss, Science 283 (1999) 1676.
[74] M. Ehrenberg, R. Rigler, Chem. Phys. 4 (1974) 390.
[75] D. Magde, E. Elson, W.W. Webb, Biopolymers 13 (1974) 29.
[76] S.T. Hess, S. Huang, A.A. Heikal, W.W. Webb, Biochem. 41 (2002) 697.
[77] P. Schwille, Cell. Biochem. Biophys. 34 (2001) 383.
[78] M. Gosch, R. Rigler, Adv. Drug Delivery Rev. 57 (2005) 169.
[79] R. Machan, T. Wohland, FEBS Lett. 588 (2014) 3571.
[80] Y. Chen, J.D. Muller, P.T.C. So. E. Gratton, Biophys. J. 77 (1999) 553.
[81] L.N. Hillesheim, J.D. Muller, Biophys. J. 89 (2005) 3491.
[82] L.N. Hillesheim, J.D. Muller, Biophys. J. 85 (2003) 1948.
[83] Y. Chen, L.-N. Wei, J.D. Muller, Biophys. J. 88 (2005) 4366.
[84] P. Kask, K. Palo, D. Ullmann, K. Gall, Proc. Natl. Acad. Sci. USA 96 (1999) 13756.
[85] S. Preus, L.M. Wilhemsson, ChemBioChem 13 (2012) 1990.
[86] R. Roy, S. Hohng, T. Ha, Nat. Methods 5 (2008) 507.
[87] D. Magde, E. Elson, W.W. Webb, Phys. Rev. Lett. 29 (1972) 705.
[88] M. Minsky, US Patent 3, 013, 467, 1957.
[89] M. Wachsmuth, C. Conrad, J. Bulkerscher, B. Koch, R. Mahen, M. Isokane, R. Pepperkok, J. Ellenberg, Nat. Biotech. 33 (2015) 384.
[90] E.J. Ambrose, Nature 178 (1956) 1194.
[91] D.J.S. Birch, Spectrochim. Acta A 57 (2001) 2313.
[92] R. Rigler, E.S. Elson (Eds.), Fluorescence Correlation Scpettroscopy, Theory and Applications, Springer Verlag, Berlin, 2012.
[93] E.S. Elson, Biophys. J. 101 (2011) 2855.
[94] D. Nettels, I.V. Gopich, A. Hoffmann, B. Schuler, Proc. Natl. Acad. Sci. USA 104 (2007) 2655.
[95] T. Otosu, K. Ishii, T. Tahara, Nature Commun. 6 (2015) 7685.
[96] F. Scholkmann, S. Kleiser, A.J. Metz, R. Zimmermann, J.M. Pavia, U. Wolf, M. Wolf, NeuroImage 85 (2014) 6.
[97] W. Becker, The bh TCSPC Handbook, sixth ed, Becker& Hickl GmbH, Berlin, 2014.
[98] J.R. Lakowicz, G. Laczko, H. Cherek, E. Gratton, M. Limkeman, Biophys. J. 46 (1984) 463.
[99] E. Gratton, M. Limkeman, J.R. Lakowicz, B.P. Maliwal, H. Cherek, G. Laczko, Biophys. J. 46 (1984) 479.
[100] R.V. Krishnan, H. Saitoh, H. Terada, V.E. Centonze, B. Herman, Rev. Sci. Instrum. 74 (2003) 2714.
[101] B.B. Das, F. Liu, R.R. Alfano, Rep. Progr. Phys. 60 (1997) 227.
[102] C. Dunsby, P.M.W. French, J. Phys. D: Appl. Phys. 36 (2003) R207.

[103] J.C. Hebden, S.P. Arridge, D.T. Delpy, Phys. Med. Biol. 42 (1997) 825.
[104] L. Wang, P.P. Ho, C. Liu, G. Zhang, R.R. Alfano, Science 253 (1991) 769.
[105] D.A. Benaron, D.K. Stevenson, Science 259 (1993) 1463.
[106] A. Andreoni, L. Nardo, A. Brega, M. Bondani, J. Appl. Phys. 101 (2007) 024921/1-8.
[107] A. Diaspro (Ed.), Confocal and Two Photon Microscopy. Foundations, Applications and Advances, Wiley-VCH, Chichester, 2001.
[108] S.W. Paddock (Ed.), Confocal Microscopy. Methods and Protocols, Springer, Berlin, 2014.
[109] R.H. Webb, Rep. Progr. Phys. 59 (1996) 427.
[110] W.B. Amos, J.G. White, Biol. Cell 95 (2003) 335.
[111] L.C. Kelley, Z. Wang, E.J. Hagedorn, L. Wang. W. Shen, S. Lei, S.A. Johnson, D.R. Sherwood, Nat. Protoc. 12 (2017) 2081.
[112] F. Schueder, J. Lara-Gutierrez, B.J. Beliveau, S.K. Saka, H.M. Sasaki, J.B. Woehrstein, M.T. Strauss, H. Grabmayr, P. Yin, R. Jungmann, Nature Commun. 8 (2017) 2090.
[113] W. Denk, J.H. Strickler, W.W. Webb, Science 248 (1990) 73.
[114] K. Tanaka, Y. Toiyama, Y. Okugawa, M. Okigami, Y. Inoue, K. Uchida, T. Araki, Y. Mohri, A. Mizoguchi, M. Kusunoki, Am. J. Transl. Res. 6 (2014) 179.
[115] C. Lefort, J. Phys. D: Appl. Phys. 50 (2017) 42300.
[116] K. Suhling, P.M.W. French, D. Phillips, Photochem. Photobiol. Sci. 4 (2005) 13.
[117] R. Cubeddu, D. Comelli, C. D'Andrea, P. Taroni, G. Valentini, J. Phys. D: Appl. Phys. 35 (2002) R61.
[118] M. Straub, S.W. Hell, Appl. Phys. Lett. 73 (1998) 1769.
[119] S. Kumar, C. Dunsby, P.A.A. De Beule, D.M. Owen, U. Anand, P.M.P. Lanigan, R.K.P. Benninger, D.M. Davis, M.A.A. Neil, P. Anand, C. Benham, A. Naylor, P.M.W. French, Opt. Express 15 (2007) 12548.
[120] M. Bates, B. Huang, G.T. Dempsey, X. Zhuang, Science 317 (2007) 1749.
[121] W.E. Moerner, Angew. Chem. Int. Ed. 54 (2015) 8067.
[122] B. Huang, M. Bates, X. Zhuang, Annu. Rev. Biochem. 78 (2009) 993.
[123] Yu Lin, et al., PLoS ONE 10 (5): e0128135. http://dx.doi.org/10.1371/journal.pone.0128135.
[124] Piotr Dorosz, Silicon Photomultipliers Applied for Fluorescence Detection of Biomarkers in the System with Self-Calibrated Gain (Doctoral Thesis), AGH-University of Science and Technology, 2017.
[125] Mateusz Baszczyk, Chemiluminescence Detection Using Silicon Photomultiplier in Stationary and Microfluidic Systems (Doctoral Thesis), AGH-University of Science and Technology, 2017.
[126] P. Dorosz, et al., Low-power front-end asic for silicon photomultiplier, IEEE Trans. Nucl. Sci. 65 (4) (2018).
[127] M. Baszczyk, et al., JINST 024P (2018) 0218.
[128] E. Martinenghi, L. Di Sieno, D. Contini, M. Sanzaro, A. Pifferi, A. Dalla Mora, Rev. Sci. Instrum. 87 (2016) 073101.
[129] D. Tyndall, B.R. Rae, D. Day-Uei Li, J. Arlt, A. Johnston, J.A. Richardson, R.K. Henderson, IEEE Trans. Biomed. Circuits Syst. 6 (6) (2012) 562–570.
[130] A. Eisele, et al., Proc, Int. Image Sensor Workshop, 2011, pp. 278–280.
[131] W. Becker, Advanced Time-Correlated Single Photon Counting Techniques, Springer, New York, 2005.
[132] S.P. Poland, et al., Biomed. Opt. Express 6 (2) (2015) 277–296.
[133] D.-U. Li, B. Rae, R. Andrews, J. Arlt, R. Henderson, J. Biomed. Opt. 15 (1) (2010) 017006.
[134] R.M. Field, J. Lary, J. Cohn, L. Paninski, K.L. Shepard, Appl. Phys. Lett. 97 (21) (2010) 211111.
[135] D.E. Schwartz, E. Charbon, K.L. Shepard, IEEE J. Solid-State Circuits 43 (11) (2008) 2546–2557.
[136] D. Stoppa, D. Mosconi, L. Pancheri, L. Gonzo, IEEE Sens. J. 9 (9) (2009) 1084–1090.
[137] L. Parmesan, N.A.W. Dutton, N.J. Calder, N. Krstaji, A.J. Holmes, L.A. Grant, R.K. Henderson, A 256 x 256 spad array with in-pixel time to amplitude conversion for fluorescence lifetime amplitude conversion for fluorescence lifetime imaging microscopy, in: International Image Sensor Workshop Paper, 2015.
[138] M. Perenzoni, N. Massari, D. Perenzoni, L. Gasparini, D. Stoppa, IEEE J. Solid-State Circuits 51 (1) (2016) 155–167.
[139] L. Parmesan, et al., A 256 x 256 spad array with in-pixel time to amplitude conversion for fluorescence lifetime imaging microscopy, in: International Image Sensor Workshop - Vaals, Netherlands, 2015.
[140] J. Richardson, et al., A 32x32 50ps resolution 10 bit time to digital converter array in 130 nm cmos for time correlated imaging, in: Proceedings of the IEEE Custom Integrated Circuits Conference, CICC 2009, San Jose, California, USA, 13-16 September, 2009, http://dx.doi.org/10.1109/CICC.2009.5280890.
[141] L. Perenzoni, et al., IEEE J. Solid-State Circuits 51 (1) (2016) 155–167.
[142] R.M. Field, S. Realov, K.L. Shepard, IEEE J. Solid-State Circuits 49 (4) (2014) 867–880.
[143] D. Li, J. Arlt, D. Tyndall, R. Walker, J. Richardson, D. Stoppa, E. Charbon, R.K. Henderson, J Biomed. Opt. 6 (9) (2011) 096012.
[144] J. Richardson, R. Walker, L. Grant, D. Stoppa, F. Borghetti, E. Charbon, M. Gersbach, R.K. Henderson, A 32x32 50ps resolution 10 bit time to digital converter array in 130 nm cmos for time correlated imaging, in: Custom Integrated Circuits Conference, 2009. CICC'09. IEEE, IEEE, 2009, p. 7780.
[145] I.M. Antolovic, et al., Sci. Rep. 7 (2017) 44108, http://dx.doi.org/10.1038/srep44108.
[146] J. Folling, et al., Nat. Methods 5 (2008) 943–945.
[147] Y. Lin, et al., PLoS One 10 (2015) e0128135.
[148] M.G. Grafton, et al., Proc. SPIE 7929 (2011) 79290C, http://dx.doi.org/10.1117/12.874299.
[149] T. Maleki, et al., Proc. SPIE 8251 (2012) 82510C–1, http://dx.doi.org/10.1117/12.9090511.
[150] V. Krishnaswami, C.J.F. Van Noorden, E.M.M. Manders, R.A. Hoebe, Opt. Nanoscopy 3 (2014) 1.
[151] F. Huang, et al., Nat. Methods 10 (2013) 6538.
[152] A. Allevi, et al., Silicon Photomultipliers: characterization and applications, in: Photodetectors, Vol. 1, pp. 77–100, RIJEKA:InTech Web Org, ISBN: 979-953-307-350-6.
[153] R. Zimmermann, et al., Biomed. Opt. Express 4 (5) (2013) 659–666, http://dx.doi.org/10.1364/BOE.4.000659.
[154] G. Giraud, et al., Biomed. Opt. Express 1 (5) (2010) 1302–1308, http://dx.doi.org/10.1364/BOE.1.001302.
[155] F.M. Della Rocca, et al., Opt. Lett. 41 (4) (2016) 673–676, http://dx.doi.org/10.1364/OL.41.000673.
[156] F. Acerbi, et al., IEEE J. Sel. Top. Quantum Electron. 24 (2) (2018) http://dx.doi.org/10.1109/JSTQE.2017.2748927.
[157] S.V. Bogdanov, et al., Proc. SPIE 10526, Physics and Simulation of Optoelectronic Devices XXVI, 2018, p. 105262G, http://dx.doi.org/10.1117/12.2290956.
[158] J.M. Pavia, et al., Opt. Express 22 (4) (2014) 4202–4213, http://dx.doi.org/10.1364/OE.22.004202.
[159] F. Nolet, et al., IEEE Trans. Nucl. Sci. 63 (4) (2016) 2293–2299, http://dx.doi.org/10.1109/TNS.2016.2582686.
[160] T. Baba, et al., SPIE digital library, in: Proceedings of the SPIE OPTO, 2017, San Francisco, California, United States, Volume 10108, Silicon Photonics XII, 2017, p. 101080Y, http://dx.doi.org/10.1117/12.2250165.
[161] T. Al Abbas, et al., 2016 IEEE International Electron Devices Meeting (IEDM), San Francisco, CA, 2016, pp. 1–8, http://dx.doi.org/10.1109/IEDM.2016.7838372.
[162] T. Al Abbas, et al., IEEE Sens. J. 18 (8) (2018) http://dx.doi.org/10.1109/JSEN.2018.2803087.
[163] A.T. Erdogan, et al., 2017 Symposium on VLSI Circuits, Kyoto, Japan, 2017, http://dx.doi.org/10.23919/VLSIC.2017.8008513.
[164] T. Niehorster, et al., Nat. Methods 13 (2016) 257–262.
[165] J.A. Levitt, et al., J. Biomed. Opt. 20 (9) (2015) 096002.
[166] A.C. Rueck, et al., J. Biomed. Opt. 19 (9) (2014) 096005.